NOTICE

AVIS

Canada

SYSTEM IDENTIFICATION OF BLADDER HYDRODYNAMICS

Jing Zhang

Department of Biomedical Engineering

McGill University

Montreal, Quebec, Canada

A thesis submitted to the Faculty of Graduate Studies and Research

in partial fulfillment of the requirements for the degree of

Master of Engineering

supervised by

Dr. Robert E. Kearney, Professor, McGill University

July 1994

ISBN   0-315-99991-8

Canada

A *bstract*

![section divider]

Abstract

Understanding bladder mechanics and the changes caused by bladder outlet obstruction is an important task in urology. In this work, bladder mechanics are examined in terms of bladder hydrodynamics: the relation between a perturbing volume applied to the bladder and the evoked pressure change. A PC-based experimental system was built which can generate a computer-controlled perturbation volume and measure volume and pressure signals.

The bladders of six minipigs, three normal and three obstructed, were subjected to stochastic volume perturbations about different average volume levels and evoked pressure changes were measured. The hydrodynamic stiffness transfer function relating volume and pressure was calculated and described by a second-order, lumped parametric model having inertial, viscous and elastic terms. Estimates of the elastic constant (K) increased linearly with volume in both normal and obstructed animals. The rate of increase was substantially greater in the obstructed animals than in the normals. Consequently, this approach shows promise for distinguishing normal and obstructed bladder mechanics.

R*ésumé*

Résumé

La compréhension des caratéristiques mécaniques de la vessie et des changements causés sur la vessie par l'obstruction de son orifice de sortie est une tâche importante en urologie. Cette thèse examine les caratéristiques mécaniques de la vessie en fonction de ses caratéristiques hydrodynamiques: la relation entre une perturbation de volume appliquée sur la vessie et le changement de pression résultant. Un système expérimental, basé sur un ordirateur PC, a été construit pour générer une perturbation de volume controllée par ordinateur et pour mesurer et enregistrer les signaux de volume et de pression.

Les vessies de six cochonnets, trois normales et trois obstruées, ont été soumises à une perturbation volumétrique aléatoire superposée à un niveau volumétrique constant, et les changements de pression produits ont été mesurés. La fonction de transfert de la rigidité hydrodynamique reliant volume et pression a été calculée et caractérisée par un modèle (lumped) deuxième ordre, avec les paramètres d'inertie, de viscosité et d'élasticité. Les valeurs estimées de la constante d'élasticité (K) augmentent linéairement avec le niveau tonique pour les vessies normales et obstruées. L'augmentation est substantiellement plus prononcée pour les spécimens obstrués que normaux. En conséquence, cette approche donne de bons espoirs pour distinguer les vessies obstruées et normales.

*A*ckpowledgments

Acknowledgments

I wish to express my appreciation to my supervisor Dr. Robert E. Kearney for his guidance, help and encouragement during my studies and my thesis work.

I am greatly indebted to Dr. George Kiruluta and Ms. Doris Greinke, whose work on animal model development and animal surgical preparation for every experiment made this research possible.

I also wish to thank Dr. Ian W. Hunter for providing the oscillatory pump.

Thanks to James P. Trainor for help in building the experimental system, to David T. Westwick for help in computer skills, to Yangmin Xiu for many valuable discussions, to Luckshman Parameswaran, Michael Steszyn and Jan Duha for help in transporting equipment and proofreading my manuscripts. Thanks also go to all other friends and colleagues in Dr. Kearney's Lab and the Department of Biomedical Engineering, McGill University for pleasant, friendly and academic atmosphere.

Finally, I would like to thank my husband, Kenong Wu, for love, help and encouragement.

TC

Table of Contents

1.

Introduction

1.1. Research Goal

Bladder outlet obstruction, due to benign prostatic hyperplasia (BPH), occurs frequently in men after middle age. Decisions regarding the surgical treatment of BPH and outcome prediction are currently based on symptomatic evidence of outflow obstruction (hesitancy, poor stream, terminal dribbling, frequency & nocturia, urgency and incontinence) and retention of urine.

Attempts to develop objective diagnostic measures of outlet obstruction on the basis of urodynamics have examined the effects of obstruction on patterns of urinary flow, bladder pressure and pressure/flow combinations. However, these output measures depend on the properties of both the urethra and the bladder itself. These two components must be separated in order to diagnose outlet obstruction.

In this research we will focus on quantifying the effects of obstruction on the bladder mechanics.

1.2. Methodology

Bladder muscle mechanics have been assessed by defining force-length and force-velocity relationships of bladder strips. Unstimulated bladder muscle behaves like a passive viscoelastic substance. The passive length-tension curve is a measure of the muscle's elasticity while the velocity-tension curve indicates the muscle's viscosity. In addition to using bladder strips, bladder wall mechanics also can be estimated in the intact bladder in terms of bladder hydrodynamics: the relation between a perturbing volume applied to the bladder and the change evoked in the pressure. Volume increases will strain the wall, developing a stress which determines a pressure depending on the geometry of the bladder.

System identification is the branch of engineering science which deals with the problem of determining mathematical models of a system's behavior through an analysis of the dynamic relation between its inputs and outputs. This approach has been used successfully for many years to study the dynamic properties of the human motor neuromuscular control system. We propose to use this approach to study bladder hydrodynamics.

1.3. Thesis Overview

This thesis is organized in five chapters as follows: Chapter II introduces the background knowledge about function of urinary bladder, animal models, several parameters developed in urodynamic research for assessing obstruction and provides the motivation of this work. This chapter also reviews the literature about modeling the bladder as a whole organ, information flow in the peripheral

neuromuscular system controlling the bladder wall muscle, the mechanism underlying bladder hydrodynamics, and the system identification approach.

Chapter III describes an experimental system that was designed and built for system identification of bladder hydrodynamics. It delivers a random volume perturbation to bladder and measures perturbation volume and pressure response.

Chapter VI describes the experimental methods including the subjects, apparatus, paradigms, stimuli and treatment of the data. The results of experimental studies are also presented.

Chapter V includes a summary of the contributions made by this work, its limitations and makes recommendations for further work.

2.

Literature Review

2.1. Anatomy and Physiology of Urinary Bladder

2.1.1. Anatomy

The *urinary bladder* is a midline structure providing a reservoir for urine. Urine passes from the renal pelvis through the ureters into the urinary bladder (Figure 2-1(a)). Urine is stored in the bladder until it is allowed to flow out through the urethra in the process of urination (micturition).

The *anatomic relationships* vary somewhat, depending upon the age of the patient and the degree of distention (Figure 2-1 (b)). The empty bladder is roughly divided into a bladder neck, trigone, bladder base, apex, and the superior and lateral surfaces. The base or posterior wall is bounded posteriorly by the rectum in the male and the anterior vaginal wall and cervix in the female. The anterior surface of the bladder is bounded by the pubic symphysis and posterior rectus sheath. The lateral walls of the bladder are bounded by the paravesical structures and the lateral pelvic wall. The urinary bladder is totally

lined by transitional epithelium which covers an interlacing network of smooth muscle fibers. There is loose areolar tissue surrounding the external surface of the bladder.

The *nerves* innervating the bladder are via the pelvic parasypathetics (pelvic splanchnic nerves) and sympathetic fibers from the hypogastric plexus as well as sensory somatic fibers from the pudendal nerves.

The *wall of the bladder* is composed of four coats (see Figure 2-2(a)): serous, muscular, submucous and mucous coats:

The **serous coat** (tunica mucosa) is a partial one and is derived from the peritoneum. It invests the superior surface and the upper parts of the lateral surfaces, and is reflected from these on to the abdominal and pelvic walls.

The **muscular coat** (tunica muscularis) consists of three layers of smooth muscle fibers: an external layer, composed of fibers having for the most part a longitudinal arrangement, named **detrusor urinae muscle**; a thin middle layer, in which the fibers are arranged in a circular manner and form **sphincter vesicae**, and a thin internal layer, in which the fibers have a general longitudinal arrangement (see Figure 2-2 (b)).

The **submucous coat** (tela submucosa) consists of a layer of areolar tissue connecting together the muscular and mucous coats and intimately united to the latter.

The **mucous coat** (tunica mucosa) is thin, smooth, and of a pale rose color. It is continuous above through the ureters with the lining membrane of the renal tubules, and below with that of the urethra.
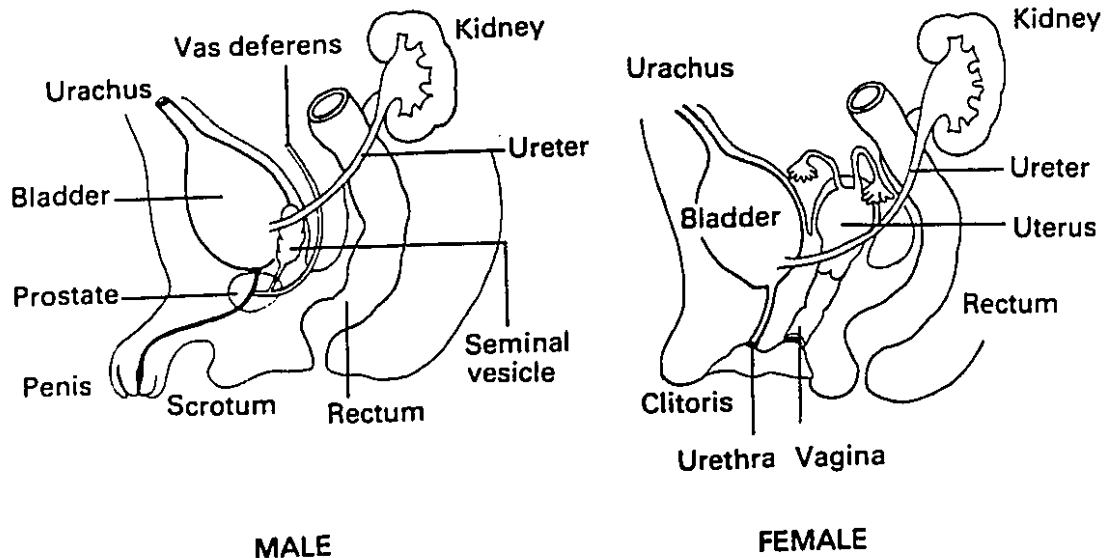
Figure 2-1: (a) Urine flows into the renal pyramids, to the calyces and pelvis, and finally through the ureter to the bladder. The bladder empties to the exterior by way of the urethra [N. Bullock et al., 1989, P. 18]
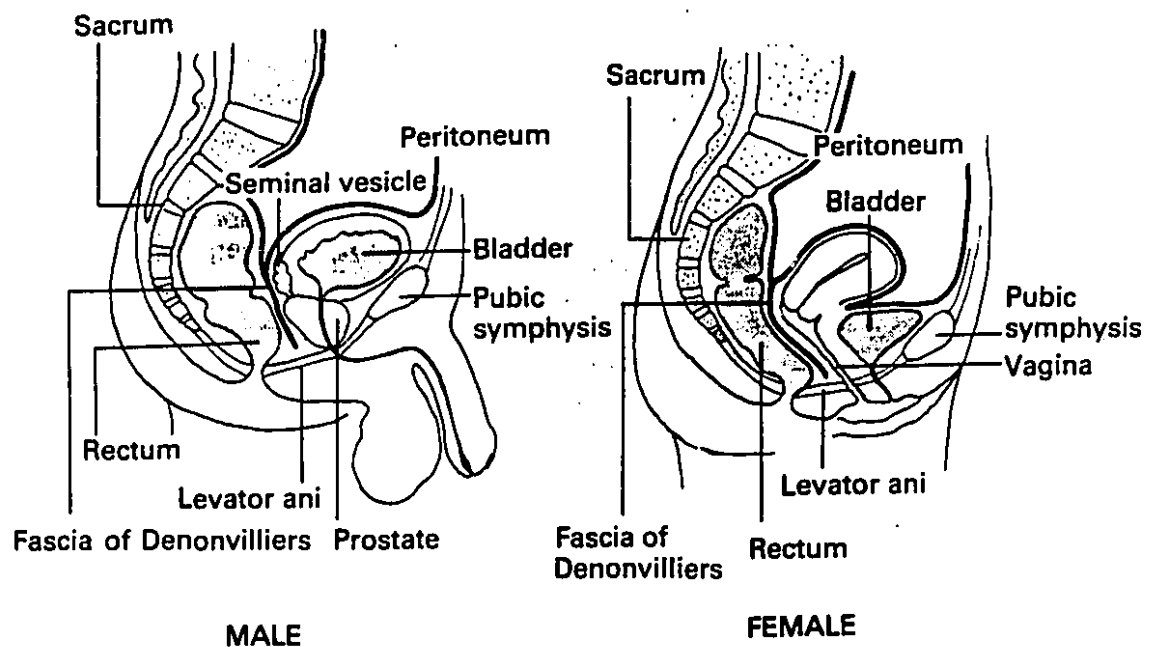
Figure 2-1: (b) Anatomical relation of the bladder [N. Bullock et al., 1989, P. 20]
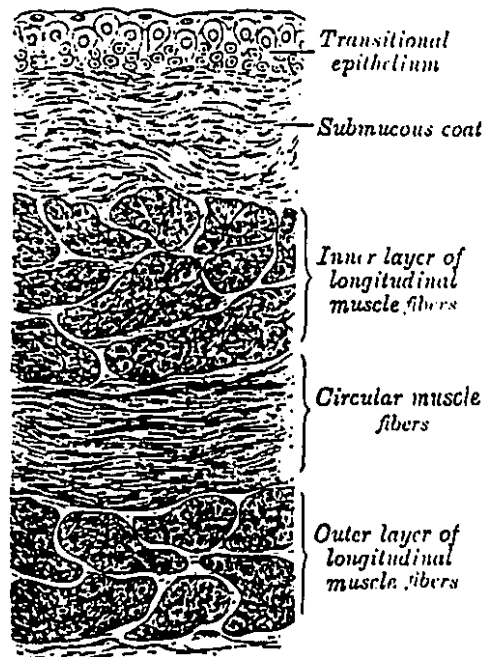
Figure 2-2: (a) Vertical section of bladder wall [H.Gray, 1966, P.1295]
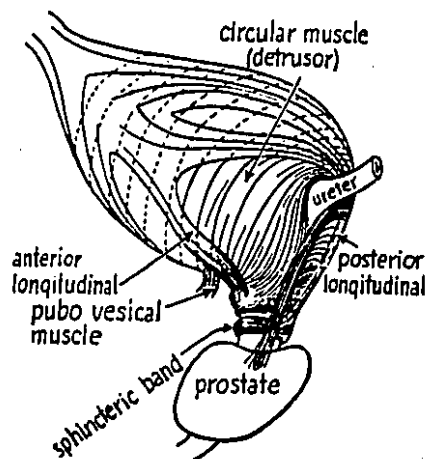
Figure 2-2: (b) Diagram of the muscle of the bladder [H.Gray, 1966, P.1295]

2.1.2. Physiology [Schauf et al. 1990]

The smooth muscle of the bladder forms the internal sphincter at the junction of the urethra with the bladder. A second, external, sphincter located at the base of the bladder is composed of skeletal muscle (Figure 2-3,a). Stretch receptors are present in the bladder and in the muscles of the internal sphincter. Filling of the bladder is detected by the stretch receptors of the bladder. The excitation of these receptors initiates a reflex contraction of the smooth muscle of the bladder; each contraction leads to another contraction because the stretch receptors are strongly excited each time the bladder contracts but does not empty (Figure 2-3,b). After several bladder contractions, the reflex pathway becomes refractory and bladder contractions cease for a period of several minutes to an hour, despite increasing bladder distention. After this period, however, the cycle is repeated.

The greater the volume of urine in the bladder, the stronger the bladder contractions become. At some point, the contractions are sufficient to open the internal sphincter and force some urine into the urethra. This initiates a second stretch reflex that inhibits the spinal motor neurons that maintain the tonic contraction of the external sphincter muscles. Urination will occur if the urethra stretch receptor input is able to prevail over the brain's control of the external sphincter. Once urination has begun, positive feedback continues as long as urine is flowing through the urethra, allowing the bladder to be completely emptied (Figure 2-3,c).
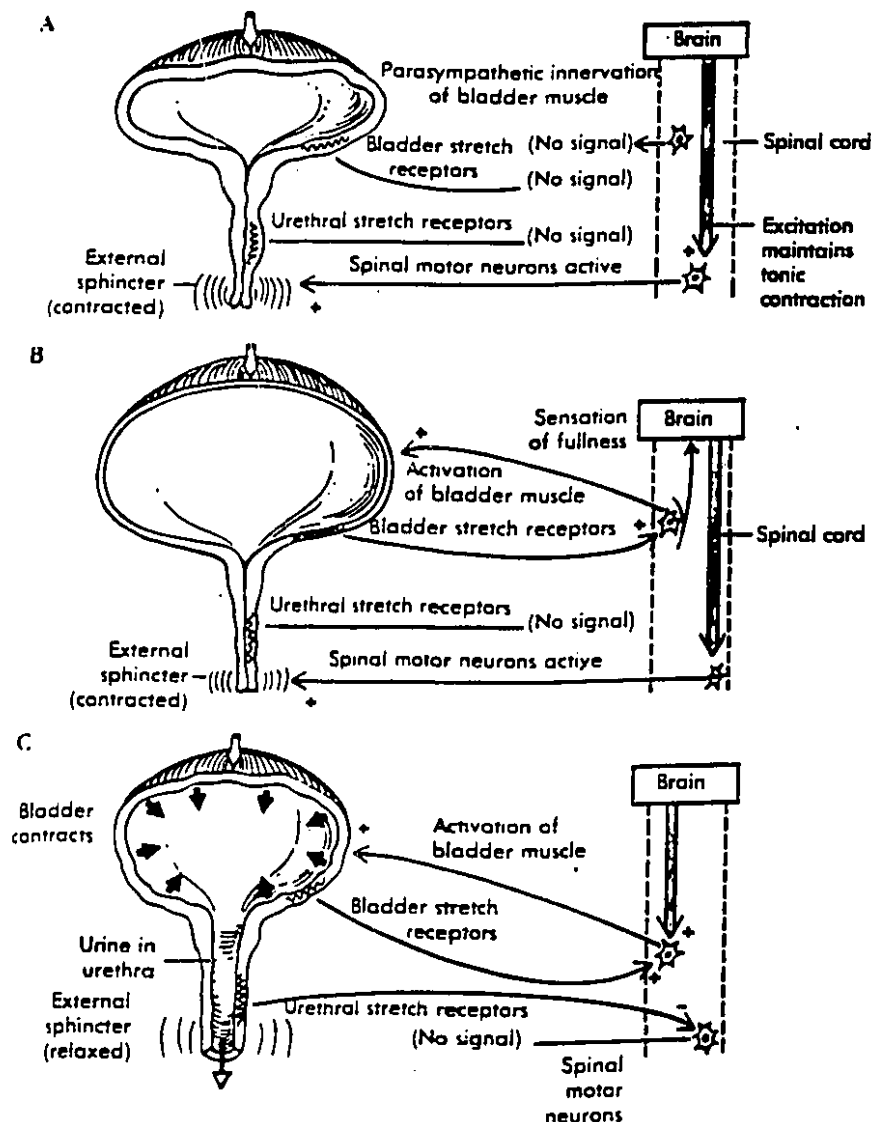
FIGURE 19-2
Micturition. -
A   The bladder contains little urine and
therefore no stretch reflex is activated. The
brain maintains the tonic drive on the motor
neurons that innervate the skeletal muscle of
the external sphincter.
B   The volume of urine in the bladder has
increased enough to activate the stretch
receptors in the bladder wall. The stretch
receptors excite the parasympathetic
innervation of the bladder, and each
contraction activates a positive feedback
loop. The external sphincter continues to be
closed in response to signals from the brain,
but the sensation of the need to void has
been felt.
C   Voluntary control of bladder emptying
occurs when the signals from the brain to
the external sphincter motor neurons cease
and stimulation of the bladder
parasympathetic innervation occurs. This is
assisted by the stretch reflex and the
inhibition of external sphincter contraction
while urine is in the urethra.

Figure 2-3: Physiology of the bladder function [Schauf and Moffett, 1990,

P.477]

The above is a simplified description of bladder function. The requirements for normal micturition may be summarized as follows:

<u>During bladder filling and urine storage:</u>

a. Increasing volume of urine, with appropriate sensation, must be accommodated at a low intravesical pressure.

b. The bladder outlet must be closed at rest and remain so as intra-abdominal pressure increases.

c. Involuntary bladder contractions should not occur.

<u>During bladder emptying:</u>

a. A coordinated contraction of bladder smooth musculature with adequate magnitude must occur.

b. A concomitant lowing of resistance must occur at the level of the internal sphincter and the external sphincter.

c. There must be no anatomic obstruction.

Abnormality in any one of these factors will result in voiding dysfunction and/or problems in bladder emptying.

2.2. Outflow Obstruction: A Urological Disease

Obstruction of the flow of urine from the bladder may occur anywhere along the length of the urethra from the bladder neck to the external meatus. The cause of the obstruction may be structural (e.g. BPH (benign prostatic hyperplsia)) or functional (e.g. bladder neck dyssynergia).

Outflow obstruction results in characteristic changes in the bladder. The obstructed bladder may show an increased irritability during filling leading to involuntary or 'unstable' contractions (detrusor instability) which causes frequency and urgency of micturition. If the outflow obstruction goes unrecognized or untreated, the detrusor muscle may become unable to overcome the obstruction so that residual urine will remain in the bladder after voiding and predispose the patient to chronic infection. This can progress to a chronic retention of urine, with a very large capacity bladder from which only a small quantity is voided at a time.

Benign prostatic hyperplasia is the main cause of outflow obstruction in men after middle age but the degree of obstruction produced is highly variable. In the UK, 75% of men have benign nodular hyperplasia of the prostate by the age of 70 but only 10-15% require prostatectomy for relief of obstructive symptoms [Bullock, N. et al, 1989]

Surgical treatment of BPH and outcome prediction currently depend on symptoms of outflow obstruction (hesitancy, poor stream, terminal dribbling, frequency & nocturia, urgency, incontinence), retention of urine or complications such as urinary infection and stone formation. Investigations of bladder function, with the objective of finding parameters suitable for diagnosing outlet obstruction, have been conducted by many researchers. An efficient quantitative norm for diagnosing outlet obstruction has not been found yet.

2.3. The Animal Model for Outflow Obstruction Study

Animal models of obstructed bladders have been developed in pigs, dogs, and rabbits. Methods of producing obstruction include:

a. Decreasing the diameter of the exit port (external meatus),

b. Constricting the urethra,

c. Increasing the number and degree of bends in the urethra.

Animal studies reveal that an obstructed bladder undergoes rapid and extensive morphological, structural, and contractile changes which are similar to those seen in an obstructed human bladder [Melick et al. 1961; Hodson et al. 1975; Ransley and Risdon 1978; Sibley 1985] .

2.4. Quantitative, Urodynamic Investigation of Bladder Function

Urodynamic investigation is an important tool in the study of lower urinary tract function. Parameters such as: maximum urine flow rate (Qmax), urethra opening pressure (Popen), maximum detrusor pressure (Pmax), the strength of the bladder contraction (WF), and group-specific resistance factor (URA) have been tried for assessment of the obstruction. Figure 2-4 shows a set of experimental urodynamic curves and how some of the parameters are defined.
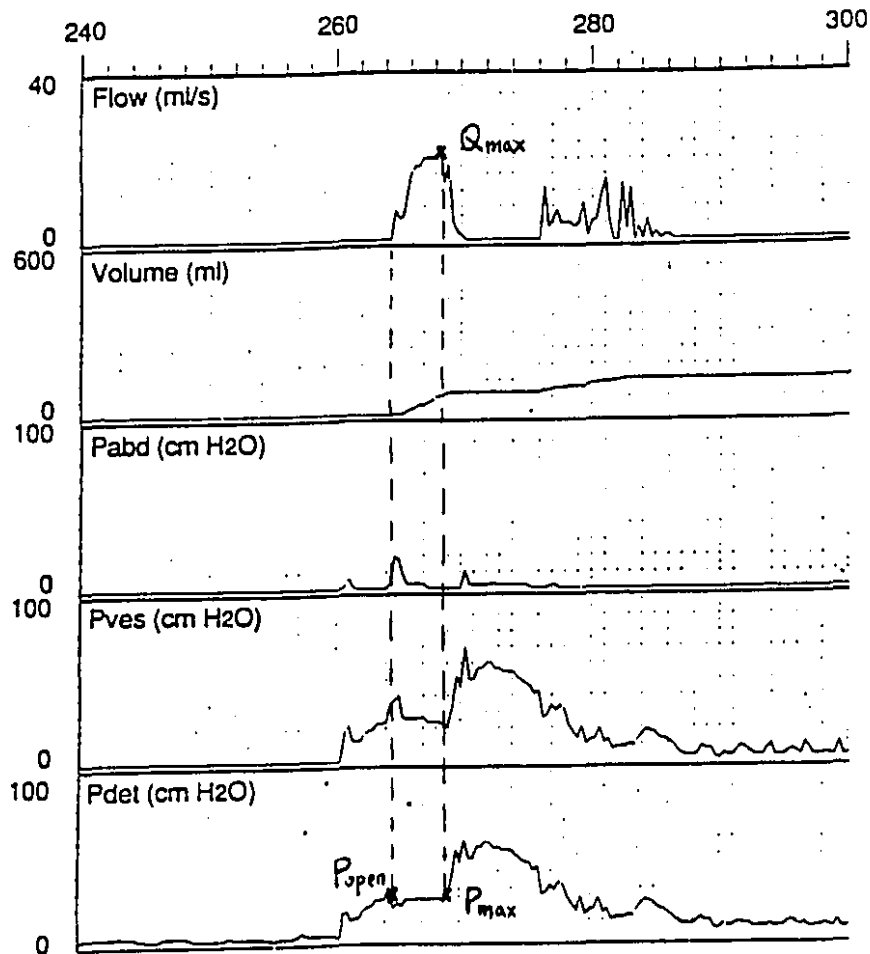
Figure 2-4: Urodynamic parameters. Q_{max} is maximum urine flow rate. Detrusor pressure (Pdet) is obtained by subtracting abdominal pressure (Pabd) from ir.travesical pressure (Pves). P_{open} is the detrusor pressure just before urinary flow starts. P_{max} is the detrusor pressure measured at peak urinary flow [Guan 1992].

2.4.1. Maximum Urine Flow Rate (Qmax)

The results of studies by Abrams and Griffiths (1979) show that patients with $Q_{max} < 10$ ml/s usually have infravesical obstruction, those with $Q_{max} > 15$ ml/s rarely have obstruction, while with $10 < Q_{max} < 15$ ml/s, it is unconfirmed. In the investigation by Abrams and Griffiths (1978) of 107 males, over the age of 55, about half of the cases could have been classified by using Q_{max}. It is also found that Q_{max} varies with sex, bladder volume, and age. The variation of Q_{max} in these different groups is being investigated [Layto and Drach, 1983].

2.4.2. Detrusor Contraction Strength (WF)

The strength of the bladder contraction can be represented by a combination of the detrusor pressure (P_{det}), the flow rate (Q) and the bladder volume (V_{bl}) according to the formula (Griffiths 1986):

$$\dot{WF} = \frac{(P_{det} + a)(V_{det} + b) - ab}{2} \qquad 2.1$$

where

$$V_{det} = \frac{Q}{2\left(\frac{3(V_{bl} + V_t)}{4\pi}\right)^{\frac{2}{3}}}$$

V_{bl} may be calculated from the urinary flow curve and residual urine in the bladder. V_t, a, and b are constants equal to 10ml, 25cmH$_2$O, and 6ml/s respectively. The units of WF are watts/m^2 and can be considered as a modified version of the mechanical power developed by the contracting bladder, or alternatively as an estimate of the isometric detrusor pressure. The value of WF varies throughout the course of micturition. During normal, residual urine free, voiding it

rises slowly attaining its maximum value when the bladder is nearly empty. If there is residual urine, it falls prematurely to a low value before the bladder is empty. The value of WF corresponding to peak flow is taken as representative of the voiding (Figure 2-5).

(a)　　　　　　　　　　　　　　　　　(b)
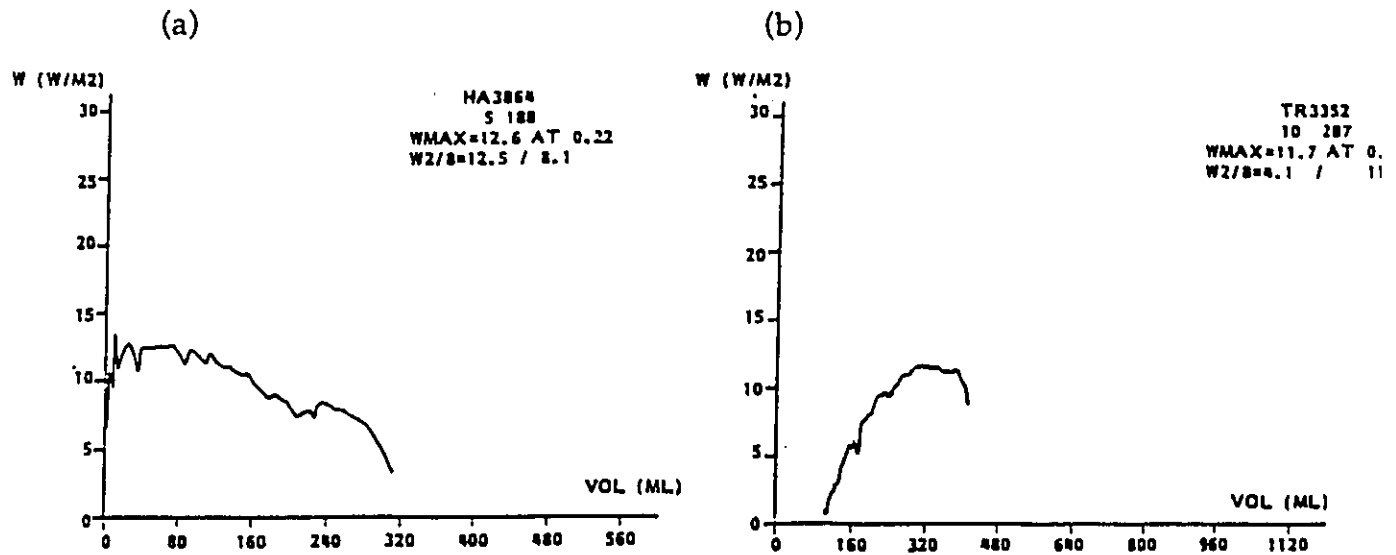
Figure 2-5: (a) Plots of WF against the bladder volume for a normal, residual-free voiding. The beginning of voiding is at the right-hand side of the curve. WF rises slowly to the maximum value near the end of voiding. (b) Voiding with residual urine. As the bladder empties the strength of the contraction fades and voiding ceases when the bladder volume is about 100ml [Griffiths et al. 1989].

2.4.3. Group-Specific Urethral Resistance Factor (URA)

Urethral Resistance R is calculated from the maximum detrusor pressure (P_{max}) and maximum urine flow rate (Q_{max}) [Malkowics et al. 1986] based on the assumption that the urethra is a rigid tube. Thus,

$$R = \frac{P_{max}}{Q_{max}^2}$$
2.2

15

a value of R smaller than 0.5 is rather arbitrarily considered to be a normal urethral resistance.

Passive Urethral Resistance Relation (PURR) was developed based on the concept that the urethra is a distensible tube [Schafer, 1985]. The PURR is defined by the part of the pressure/flow plot from the beginning of the flow to the peak of flow. It is fitted with the curve suggested by Schafer (see Figure 2-6):

$$P_{det} = P_{open} + \frac{Q^2}{c} \qquad\qquad 2.3$$

where P_{det} is the detrusor pressure and Q the urine flow rate. P_{open} represents a "urethral opening pressure" and c is related to an "effective cross-sectional area".

For adults, with no obstruction both P_{open} and $1/c$ tended to be low, while with obstruction both tended to be elevated. P_{open} and $1/c$ were therefore positively correlated. If the correlation was perfect, either one of them alone could be used to quantify the urethral resistance, the other being superfluous. The approximate relation was:

$$\frac{1}{c} = d \cdot P_{open}^2 \qquad\qquad 2.4$$

With pressure expressed in cmH_2O and flow rate in ml/s, the constant d had the approximate value : ·

$$d = 3.8 \times 10^{-4} \qquad\qquad 2.5$$
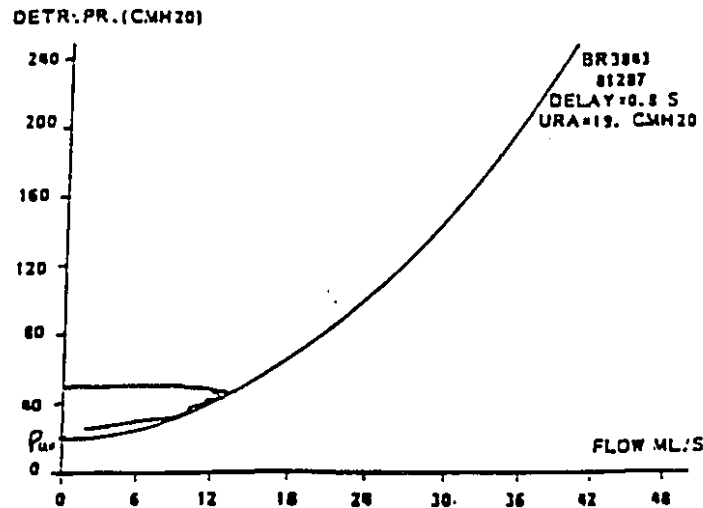
Figure 2-6: Pressure/flow plot and corresponding curve of the form suggested by Schafer (1985). In this case the curve has been fitted through the peak flow point by the computer, using the empirical relation between P_{open} and $1/c$. The resulting value of P_{open} (=19 cmH_2O) is the representative value of URA for this micturition [Griffiths et al. 1989].
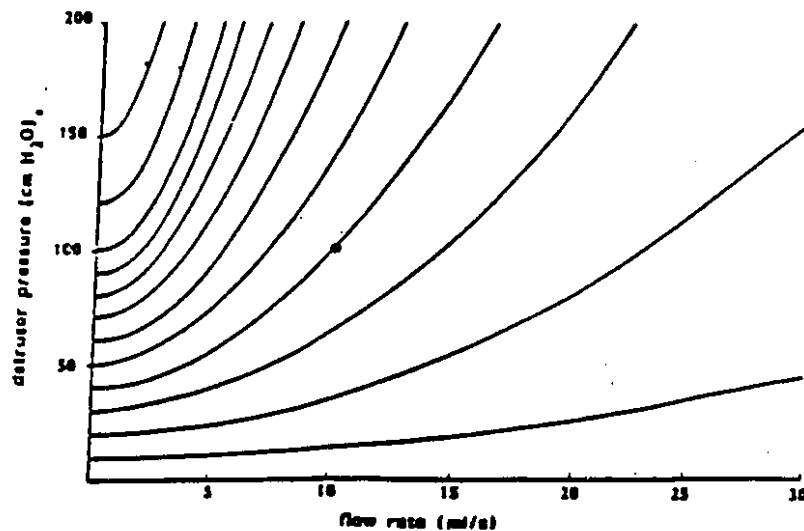
Figure 2-7: Pressure/flow curves for various constant value of URA from 10 to 150 cmH_2O. The filled circle represents a moment of voiding when the detrusor pressure is 100 cmH_2O and urine flow rate is 10 ml/s. This point lies on the curve for URA=40 cmH_2O, which is therefore the value of the urethral resistance at this moment [Griffiths et al. 1989].

17

These equations define a series of curves which show the average pressure/flow plots for different values of P_{open} (Figure 2-7). Each curve represents a different urethral resistance, and the value of P_{open} for the curve can be taken as the corresponding resistance factor. Any pair of pressure/flow values occurring during a micturition can be represented by a point in Figure 2-7 . The value of P_{open} for the curve on which the point lies represents the Urethral Resistance Factor (URA). URA can thus be calculated for any pair of pressure/flow values by solving the above equation for P_{open}:

$$URA = P_{open} = \frac{\sqrt{1+4dQ^2 P_{det}} - 1}{2dQ^2} \qquad 2.6$$

The units of URA are the same as those of pressure, i.e. cmH_2O.

Using the value of URA at peak flow, different voidings can be ranked according to the degree of urethral resistance, and changes or differences in urethral resistance among groups of adult patients can be identified.

2.5. Motivation

Attempts to develop objective diagnostic measures of outlet obstruction on the basis of urodynamics have examined the effects of obstruction on patterns of urinary flow, bladder pressure and pressure/flow combinations. However, these output measures depend on the properties of both the urethra and the bladder itself. These two components must be separated in order to diagnose outlet obstruction.

In this research we hope to characterize bladder mechanical properties and to quantify the effects of obstruction on the bladder mechanics.

2.6. Mechanical Properties of the Bladder Wall

The bladder, composed of passive (collagen, elastin) and active (smooth muscle) elements in an unknown functional relationship, demonstrates some simple mechanical properties both in vitro and in vivo [Remington and Alexander, 1955; Coolsaet et al, 1975; van Mastrigt et al, 1978].

2.6.1. Rate Dependency

The bladder wall undergoes considerable strain during physiological filling and investigations have shown that, among other factors, the speed with which the wall is strained (or elongated) determines the force developed. Very slow strain will cause a smaller and slower increase in force than fast strain (Figure 2-8).

2.6.2. Time Dependency

When length is kept constant after a fast strain, a decrease in the force occurs (Figure 2-8). The amount of decrease is dependent on the previous rate of strain.

2.6.3. Hysteresis

The relation between bladder volume and mean bladder pressure is found to have a characteristic shape like the one in Figure 2-9. A bladder always displays some hysteresis on deflation, and the pressure increases linearly over a region of midrange volume, but when the elastic limit of a bladder is reached, the gradient of the pressure rise is very steep and the rise is not a linear function of the volume.

A

B
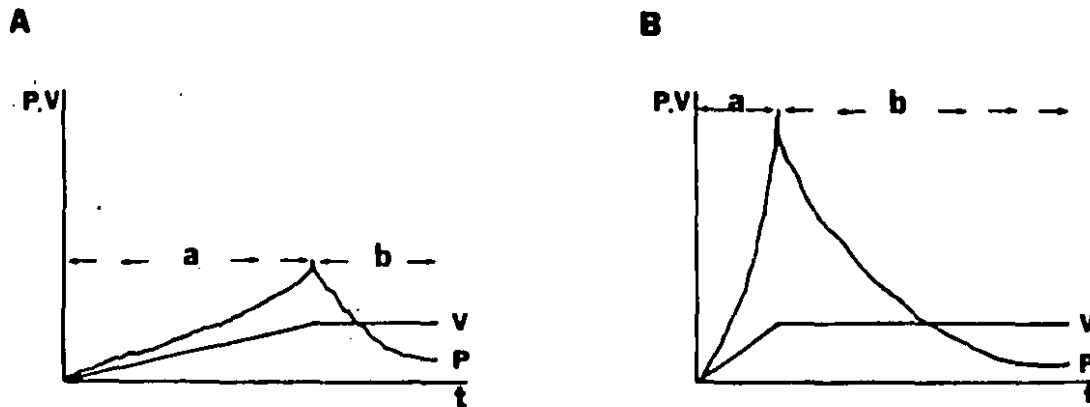
Figure 2-8: Pressure in the bladder is dependent on the rate of filling. Fast filling (B) results in higher pressure increase than slow filling(A). As soon as the filling is stopped, the pressure decreases in relation to time. The amount of decrease is dependent on the previous rate of strain.a=volume increases, b=constant volume.[B.L.R.A. Coolsaet, 1985]
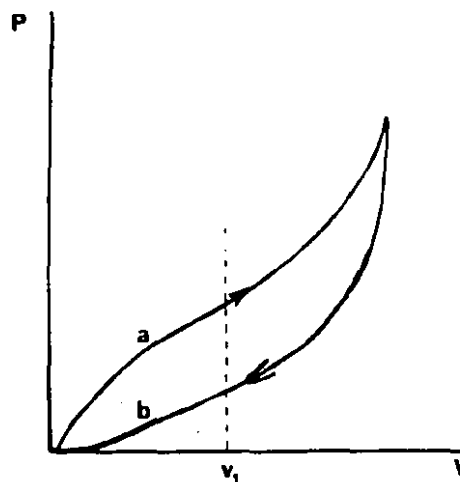
Figure 2-9: Pressure-volume curve during fluid injection(a) and withdrawal(b) shows a hysteresis loop. The pressure at volume v1 is higher during filling than during withdrawal.[B.L.R.A. Coolsaet, 1985]

2.7. Bladder Model Considerations

The most widely accepted model of muscle mechanics was originally proposed by Hill (1938) (Figure 2-10). This three-element model included a series elastic element (SEE), a contractile element (CE), which represented the properties of the active muscle, and a parallel elastic element (PEE), which represented its passive viscoelasticity.
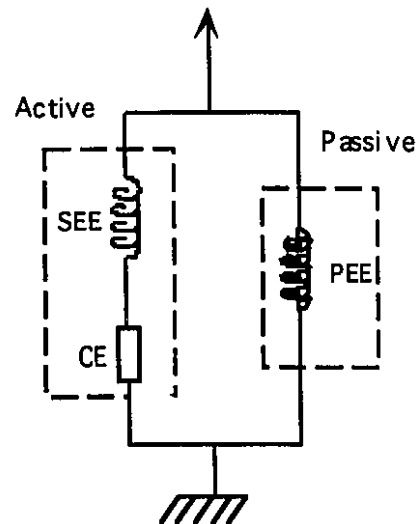
Figure 2-10: Schematic representation of active and passive limbs of Hill's 3-element model of muscle mechanics [Hill, A.V., 1938]

Since Hill's original three-element model, many articles have attempted to characterize the individual elements of Hill's model independently. For example, the steady-state, force-velocity relationship in a tetanic contraction (Hill's hyperbolic relationship [Hill, A. V., 1938]) has been used to characterize the CE. The SEE, thought to represent the elasticity of the elements transmitting the force generated by the CE, has been assessed by measuring the change in active force during quick releases [Van Mastrigt, R., B. L. R. A. Coolsaet and W. A. Van Duyl, 1978] or by measuring dynamic stiffness during

small-amplitude oscillations at frequencies where the CE was expected to remain virtually unchanged [Rack, P. M. H., 1966]. Finally, the properties of the PEE have been traditionally measured in simple force-length studies of passive muscle. Although these tests have characterized the elements of Hill's model separately, they have not successfully characterized the viscoelastic properties of muscle as whole.

Rate, time dependency, and hysteresis have been explained in the past as active phenomena due to contraction and relaxation of the smooth muscle cells, probably under control of the central nervous system. However, from the investigations of Alexander and Remington (1955), Kondo et at. (1972), Coolsaet et al. (1973, 1975) and Van Mastrigt et al. (1978), it has become clear that these characteristics of the bladder wall are not necessarily due to active properties of smooth muscle; inactive elements (polymers) and passive tissue show qualitatively the same behavior, which is known as viscoelasticity. The fact that bladder behavior can be described and analyzed by means of a passive model does not necessarily mean that active mechanisms are not involved as well. Smooth muscle cells are elongated when the bladder is stretched and their properties will surely affect the parameters studied in the passive model [Coolsaet, 1977]. However, in-vitro experiments have shown that in normal bladders, active elements influence only rapidly changing variables, and have little effect on the changes induced by slow strain.

2.8. Mechanisms Underlying Bladder Hydrodynamics

Venegas (1991) and Woolfson et al. (1991) first estimated the mechanical properties of bladder muscle by investigating bladder hydrodynamics: the dynamic relation between bladder volume and pressure. This provides a method to investigate the dynamic properties of the bladder as a whole organ. The following information flow diagram describes how the bladder hydrodynamic properties are related to the bladder muscle properties (Figure 2-11). It is drawn taking volume as the input and pressure as the output. Volume increases will strain the wall developing a stress; the resulting pressure will depend on the geometry of the bladder.

2.8.1. Muscle Mechanics

We consider mechanics of the bladder wall as a whole including the properties of both skeletal muscle and smooth muscle. Pressures due to bladder wall mechanics are likely to contribute to bladder hydrodynamics whenever muscles are activated. Two distinct mechanisms interact to determine the force developed by a muscle: contractile mechanics and activation dynamics.

Contractile Mechanics

Contractile mechanics determine the stress generated in response to strain when the level of activation remains constant. This stress may be caused by both strain of smooth muscle cell and skeletal muscle in the bladder wall. As noted above, this is a nonlinear function of the level of contraction, the displacement amplitude and direction (elongation/release), its velocity, and several other factors [Coolsaet et al., 1975, Mastrigt et al, 1978, Coolsaet 1985].

Activation Dynamics

Changes in muscle force can also occur as a result of reflex and/or voluntary changes in the level of activation, or smooth muscle spontaneous action.
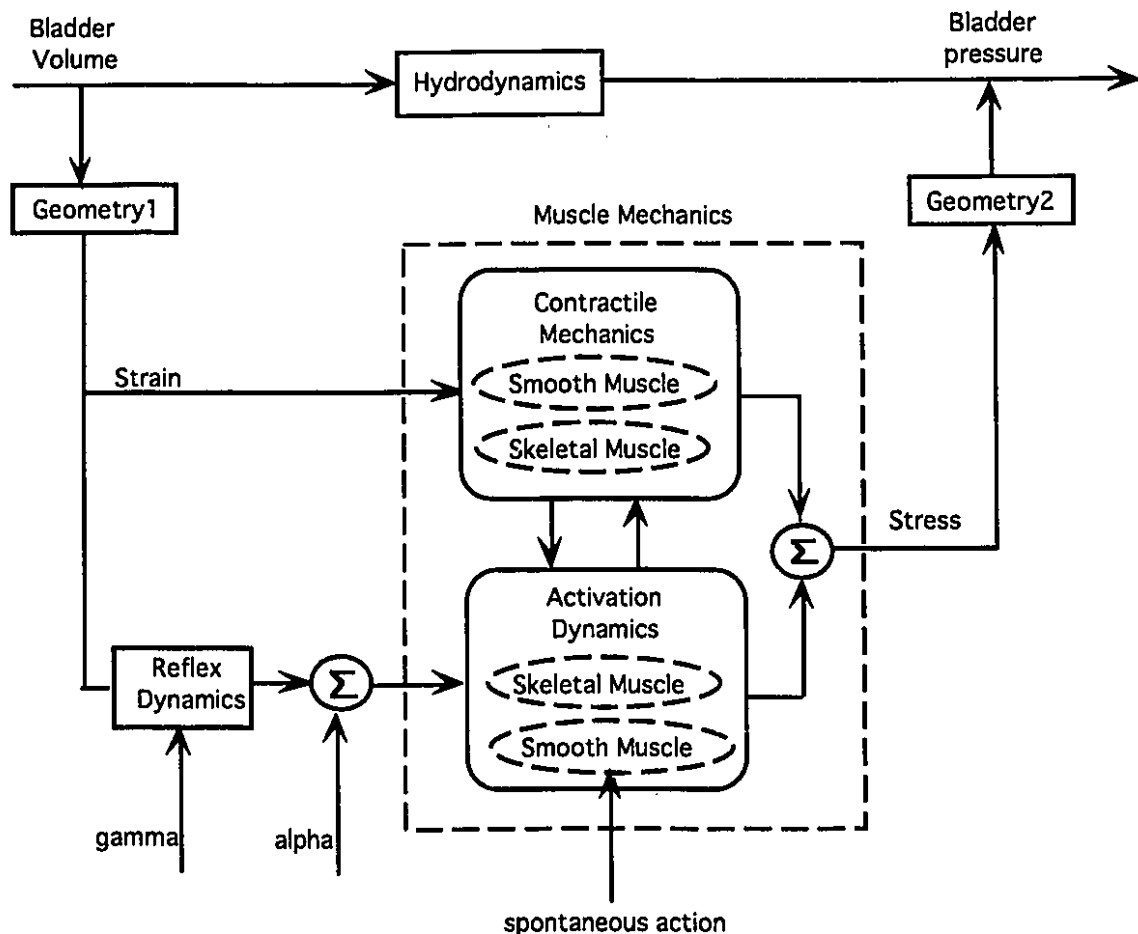
Figure 2-11: Information flow for bladder hydrodynamics
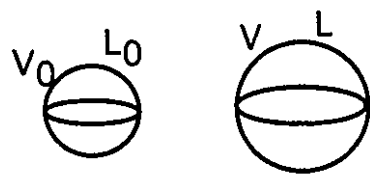
Interactions Between Contractile Mechanics and Activation

Under physiological conditions muscle length and level of activation will change at the same time, and so interactions between the contractile mechanics and the activation dynamics will occur. The nature of these interactions is not fully understood. Quasi-linear

models in which the contractile mechanics and activation dynamics are treated as independent processes are adequate for small perturbations about an operating point, but cannot deal with more general conditions involving large changes in position or activation level [Kearney, R.E. and Hunter, I.W. 1990]

2.8.2. Geometry1 (Relation Between Muscle Strain and Bladder Volume)

The first geometric block gives the relation of volume to strain. Assuming that the urinary blabber is a thick-walled hollow sphere this can be described as follows:

$$\varepsilon = \frac{\ell - \ell_0}{\ell_0} = \frac{\ell}{\ell_0} - 1 = \left(\frac{V}{V_0}\right)^{\frac{1}{3}} - 1 \qquad 2.7$$

Where: ε = strain,

V = volume,

V_0 = unstrained volume of the bladder,

l_0 = unstrained circumference of the bladder,

l = circumference of the bladder.

2.8.3. Geometry2 (Relation Between Muscle Stress and Bladder Pressure)

A second geometric block relates stress to pressure. If it could be assumed that the urinary bladder is a thin-walled hollow sphere then the Laplace formula would apply. This formula expresses tension as force per unit length:

$$T = \frac{pR}{2} \qquad 2.8$$

Where: T = tension (N/m),

p = pressure (N/m^2),

R = radius (m).

However, because we want to consider changes in wall thickness, the Laplace formula cannot be used. To express tension as force per unit surface, the tension defined by the Laplace formula must be divided by wall thickness:

$$\sigma = \frac{pR}{2d} \qquad\qquad 2.9$$

Where: σ = stress (N/m^2),

d = wall thickness (m).

Assuming tissue volume remains constant we can set:

$$d \cdot 4\pi R^2 = V_t = cons\tan t \qquad\qquad 2.10$$

Where: V_t = tissue volume (m^3).

Substituting equation 2.10 into 2.9 yields:

$$\sigma = \frac{3pV}{2Vt} \qquad\qquad 2.11$$

Where: V = intraluminal volume (m^3).

The tissue volume can be measured after an experiment.

2.9. Relevant Studies

2.9.1. Hydrodynamic Changes with the Level of Detrusor Activity

According to the mechanisms underlying bladder hydrodynamics described above, we consider the study of Venegas, J.G.(1991) and Woolfson et al. (1991) as an investigation of how bladder

hydrodynamic stiffness changes with the level of the activation. Isometric contraction of the detrusor was triggered by urethral perfusion and activation level was related to the mean pressure in the bladder P_{det}. They found the magnitude of bladder hydrodynamic stiffness $|G|$ increased linearly with mean detrusor pressure (P_{det}). When bladder dynamic behavior was modelled by a second-order system composed of spring, dashpot and mass elements, the incremental elastance (K) and incremental resistance (R) increased linearly during isometric contraction.

2.9.2. Passive Properties of the Bladder in the Collection Phase

Mastrigt et al. (1978) studied contractile mechanics using strips of urinary bladder. The time-dependent properties of the bladder wall were explained using a visco-elastic model and were determined by relaxation tests. The length-dependent properties were shown to yield moduli, which depend biexponentially on strain and are determined by stepwise straining tests. Combination of these two properties and another two geometric blocks yielded an overall model of the passive properties of the urinary bladder in the collection phase. The model contains 14 parameters. Two geometric blocks they developed are used in this paper when we interpret the mechanisms underlying bladder hydrodynamics.

2.10. System Identification Approach

System identification is the branch of engineering science which deals with the problem of determining mathematical models of a system's behavior through an analysis of the dynamic relation between

its inputs and outputs. This approach has been successfully used for many years to study the dynamic properties of the human motor neuromuscular control system. By examining the torque generated in response to an experimentally applied pseudo-random perturbation in joint position, linear models describing joint mechanics under stationary conditions, as well as model parameters which change with important variables such as level of activation and position have been developed and characterized. More recently, time-varying and non-linear aspects of the mechanics have been examined [Kearney, R.E. and Hunter, I.W. 1990].

The analogy with joint mechanics is close: bladder mechanics may be characterized in terms of the relation between volume and pressure in exactly the same way as joint mechanics are characterized in terms of the relation between position and torque.

Experiments using stochastic inputs can characterize system dynamics with very short experimental records. Stochastic data may be used to compute nonparametric frequency response or IRFs, and determine parametric models efficiently with no a priori assumption with respect to structure. Because of these advantages, we propose to use the same method to study bladder mechanics before and during obstruction.

2.11. Objectives

The objectives of this work are to build an experimental system, to conduct experiments and collect data, to identify bladder hydrodynamic characteristics, and to provide quantitative descriptions of the effects of obstruction on bladder mechanics.

It is to be expected that linear models of bladder mechanics will depend strongly on overall bladder volume. However, in view of the efficiency of the system identification procedure, we should be able to characterize bladder mechanics quickly so that bladder volume may be considered to be constant. By repeating the identification procedure as the bladder is filled, we will be able to monitor how the bladder mechanics change with bladder volume. Such information will be useful in and of itself; comparison of the results of experiments performed before and after obstruction will provide quantitative descriptions of the effects of obstruction on bladder mechanics.

3.

Experimental System

We designed and built the experimental system shown schematically in Figure 3-1 to identify bladder mechanics. A perfusion pump (DISA 21H04) is used to fill the bladder to various volumes. The oscillatory pump delivers a computer controlled pseudo-random volume stimulus to the bladder. Bladder pressure is measured by the pressure measurement path. The system comprises the following main elements:
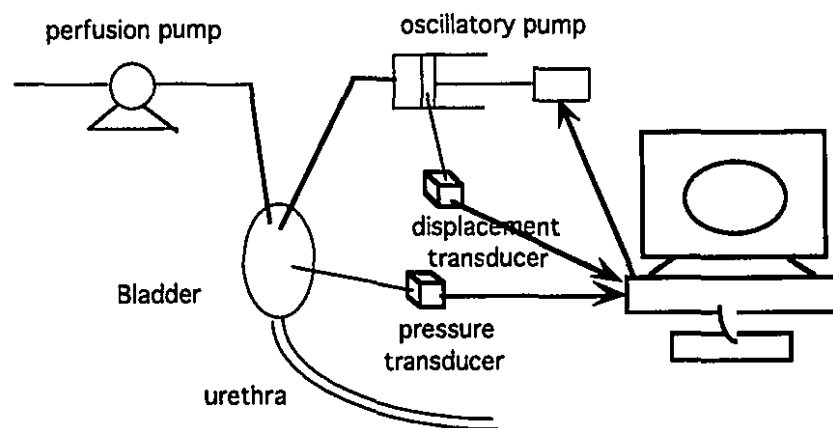
Figure 3-1: Diagram of experimental system

3.1. The Measurement System

Bladder pressure and perturbation volume are two important signals for identifying the bladder hydrodynamic system. Perturbation volume was estimated by measuring the piston's position. Position and bladder pressure pass through transducer, amplifier, anti-alias filter and A/D converter, to the computer (see Figure 3-2).
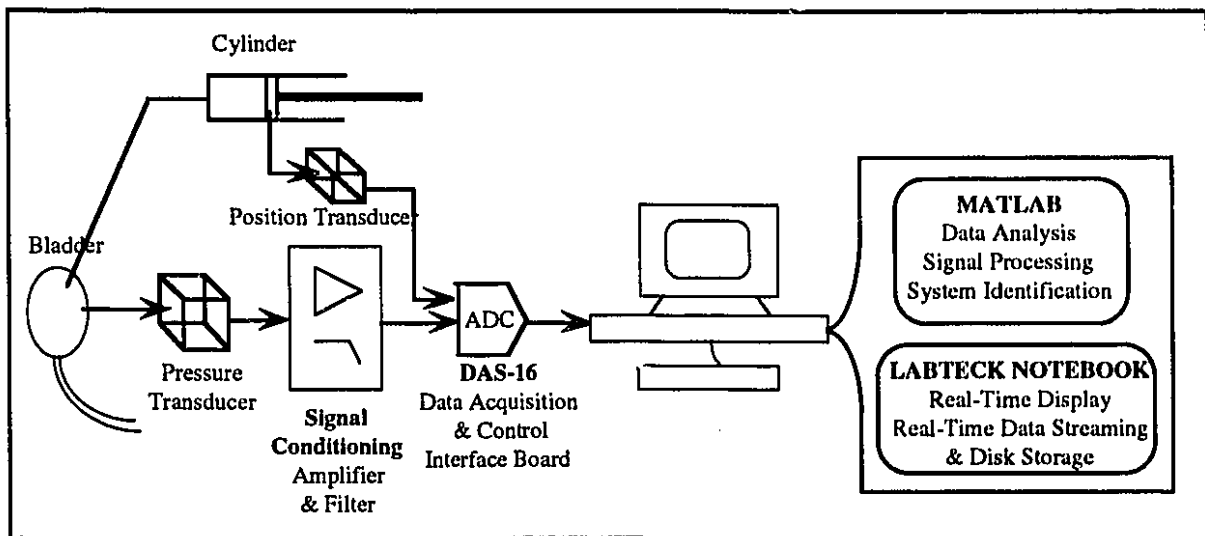
Figure 3-2: Measurement system

3.1.1. Pressure Transducer

Pressure in the bladder is sensed by a KAVLICO P612 pressure transducer with a pressure range of 0 - 15 psi (1000 cm H_2O) and bandwidth of 15Hz; other specifications are given in Appendix I. The pressure transducer is excited by +12V DC derived from a 15V DC power supply using a 12V Zener (see Figure 3-3). Since we will use low frequency volume changes to stimulate the bladder, the frequency content in pressure response will not exceed 10Hz, so the transducer's

15Hz bandwidth is adequate for this project. The maximum bladder pressure is around 100cmH$_2$O, well within the pressure range of the transducer.

3.1.2. Signal Conditioning

The output signal of the pressure transducer must be offset-compensated, amplified and band-limited before it is fed to the A/D-board for digitization. The signal conditioning circuitry contains an offset-trim potentiometer, a differential amplifier with adjustable gain, followed by a 6-pole Bessel anti-aliasing filter with adjustable cutoff frequency (see Figure 3-3).

i. Offset Compensation

The pressure transducer (Appendix I) has a pressure range of 0-15 psi corresponding to an output voltage range of 2.8-5.0V. To take full advantage of the resolution of the A/D, a offset-adjust circuit was added to transfer 2.8V to 0V for 0 psi (see Figure 3-3). The value of the potentiometer can be estimated by:

$$-12V + \frac{(2.8V - (-12V))R}{100K\Omega} = 0$$

Solving for R, we obtain

$$R = \frac{12V \times 100K\Omega}{14.8V} \approx 81K\Omega \qquad\qquad 3.1$$

ii. Differential Amplifier

The signal conditioning amplifier used in this system is standard differential amplifier circuit employing a MOTOROLA 'LM324' integrated circuit. Its purpose is to amplify the pressure signal to a level that permits good resolution after digitization. The gain is adjustable and was determined according to the experimental condition.

The pressure transducer gives a full scale (5V) output at 1,000 cmH2O. However since bladder pressure will not exceed 100cmH2O and the A/D was set at ±10V, it is appropriate to amplify by 2.5.

The gain of the integrated differential amplifier LM324 is determined by the equation

$$Gain = 1 + \frac{R_e}{75\Omega} \qquad\qquad 3.2$$

The real gain is obtained by adjusting Re to get 10V output from the amplifier for 100cmH2O pressure input. The sensitivity specified in volts is about 100mV per 1 cm H2O height. Figure 3-3 shows the circuit diagram of the differential amplifier.

The LM324 has a frequency bandwidth of about 6 KHz , well above that needed.

iii. Anti-aliasing Filter

Sampling a signal with frequency components greater than half the sampling rate will lead to a phenomenon known as aliasing in which the high frequency components in the signal appear as artifactual lower frequency components in the sampled signal. To prevent aliasing, the signal must be band limited to a value no larger than half the sampling frequency.

The band-limiting of the signal is performed by the resistive tunable, lowpass active, 6-pole Bessel filter (FREQUENCY DEVICES '746LT-1'). Its specifications are shown in Appendix II and its placement within the circuit can be seen in Figure 3-3. It should be noted that a total of six resistors of equal value, organized in three branches of two, are necessary to tune the cutoff frequency of the filter. The 1KΩ potentiometer serves to zero the output offset of the 746LT-1.
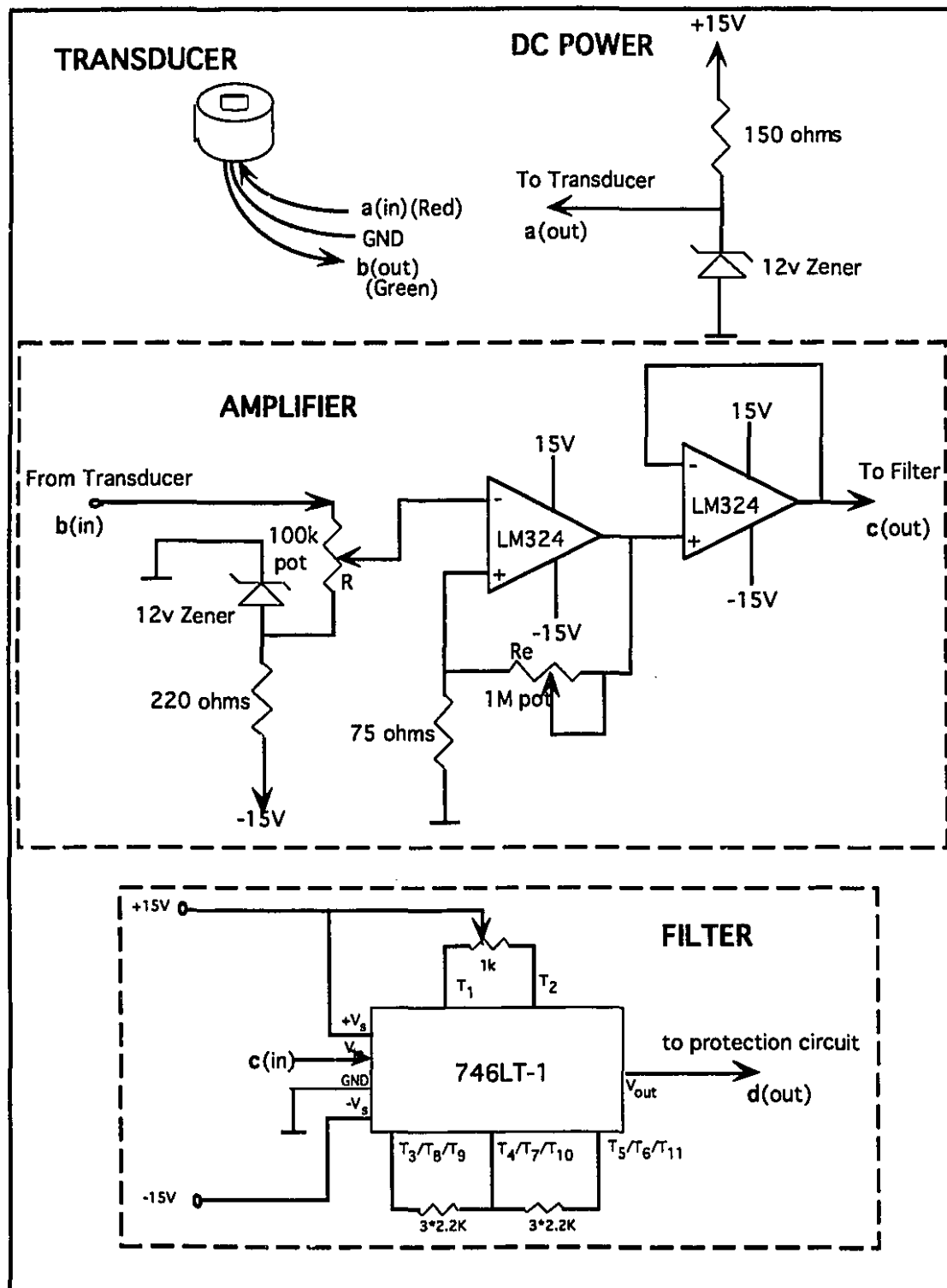
Figure 3-3: Signal conditioning

The experimental conditions were considered in order to decide on a suitable cutoff frequency. From the motor's dynamic characteristics (discussed later), we know the useful frequency content of the volume stimulus is about 0 - 4Hz. Preliminary experiments showed that the frequency content in the pressure response was no higher than 10Hz. We therefore chose 50Hz as sampling frequency and the anti-aliasing filter was set to have a cutoff frequency of 25Hz, which will also depress 60Hz noise.

The values of the tuning resistors in the anti-aliasing filters were chosen according to the equation

$$R = 2k\Omega\left(\frac{f_{c_{max}}}{f_c} - 1\right)$$ 3.3

Since the maximum cutoff frequency (f_{cmax}) was 50Hz and a cutoff frequency (f_c) of 25Hz was required. Ideally, the resistor values should be 2 kΩ, the actual values chosen from the 1% tolerance chart were 2.2 kΩ, giving a cutoff of 24 Hz.

iv. Protecting Circuit

In order to protect the DAS-16 data acquisition board from damage caused by high voltage, a protection circuit (Figure 3-4) was added after the filter output. It ensures that the input to the A/D converter will always be less than ± 10V.
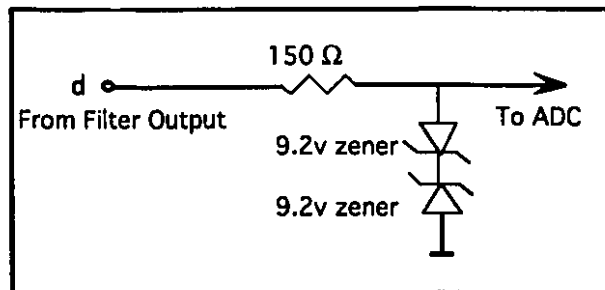
Figure 3-4: Protecting circuit

3.1.3. Volume Estimates

The perturbation pump was connected to the bladder through a 15cm long tube. The volume of perturbing water introduced into the bladder was estimated by multiplying the position of the piston which was measured by a displacement transducer (described later in Section 3.2.2) by a calibrating constant which was obtained by connecting the pump to a graduated cylinder through the same tube and finding the dynamic relation between the displacement of the piston and volume. This method of volume measurement could yield a time delay comparing with the actual volume signal and a magnitude error caused by the presence of air bubbles in the tube and/or in the cylinder. Therefore, it is required to remove all air bubbles during each experiment.

3.1.4. A/D

The DAS-16 is multifunction, high-speed, programmable, A/D, I/O expansion board for the IBM Personal Computer. Important specifications of this board are given in Table 3-1.

Table 3-1: Specifications of DAS-16

Channels	8 differential or 16 signal-ended switch-selectable
Resolution	12 bit
Input Range	±10V, ±5V, ±2.5V,±1V, ±0.5V; or 0-10V, 0-5V, 0-2V, 0-1V switch-selected.
Maximum Sample Rate	50KHZ with DMA mode
Accuracy	0.01% of reading ±1bit
Linearity	±1 bit

i. Noise Prevention

Differential input mode was used. The 8-channel differential configuration of A/D board was chosen to reduce common-mode noise picked up along transmission lines.

The ground referred signals from the protection circuit outputs were connected as shown in Figure 3-5 to minimize the noise.
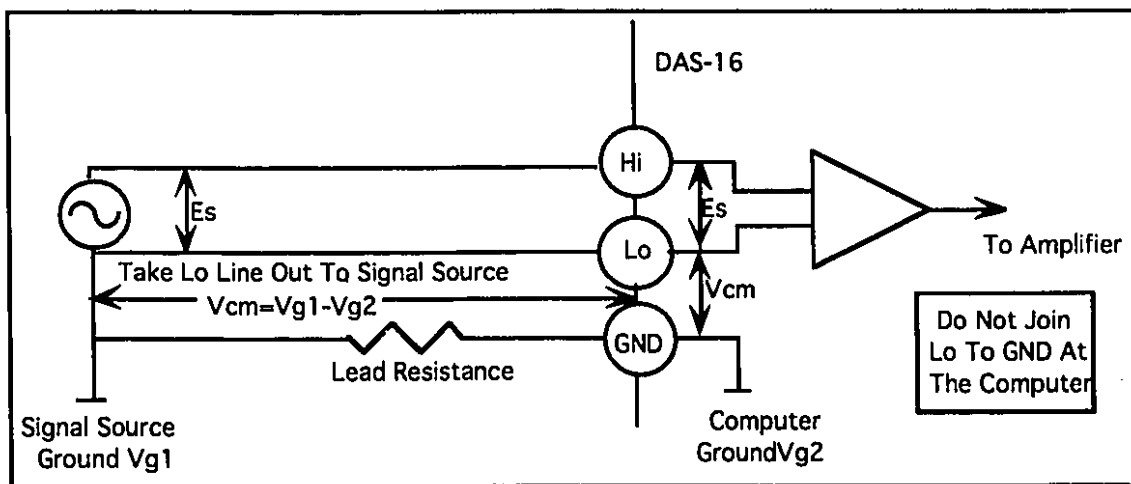
Figure 3-5: Connect a ground signal source

3.1.5. The Personal Computer

The computer used as the center of the system was Micro 486, 33MHz, 8MB RAM, 130MB hard disk, Personal Computer. Data acquisition and control was done with the LABTECH 'NOTEBOOK' package [LABTECH, 1991] and data analysis and signal processing carried out using 'MATLAB' [Mathworks, 1990].

3.2. Computer-Controlled Pump System

Figure 3-6 contains a diagram of the pump system. The core is a sevo-controlled linear motor that drives a piston in a cylinder to push/pull the water in/out the bladder. A 486 personal computer generates the command signal which controls the actuator. It is possible to apply a wide variety of arbitrary perturbations.
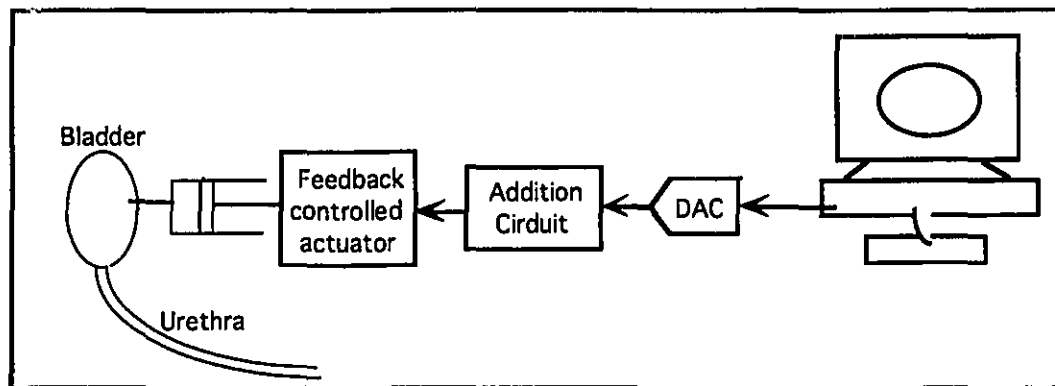
Figure 3-6: Diagram of the computer-controlled pump system

3.2.1. D/A

The computer is equipped with KEITHLEY METRABYTE DAS-16, two channel, multiplying 12-bit D/A. The DACs use a fixed, on board, -5V reference to generate 0 to 5V output and -10V reference to generate 0 to +10V. Because our requirement was to output a random bipolar waveform, a addition circuit (Figure 3-7) was used to shift the DAC's output from 0V to 10V to -5V to +5V .
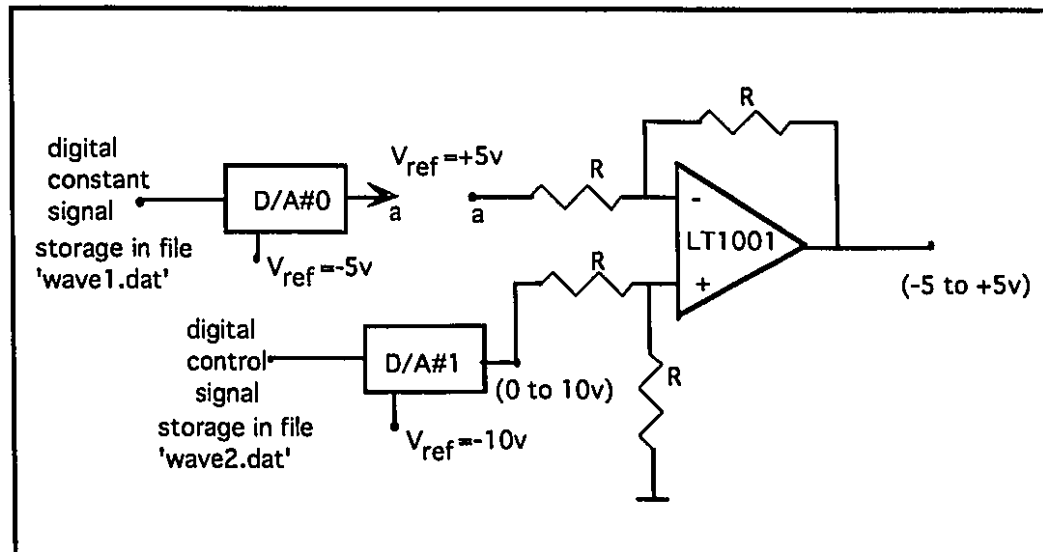
Figure 3-7: Addition circuit. Using D/A#0 and -5V on board reference to generate a constant voltage output +5V. D/A#1 and LT1001 provide a bipolar voltage signal.

3.2.2 Pump

Dr. Ian Hunter (Dept. of Biomedical Engineering, McGill University, Montreal, Quebec) built a feedback controlled pump for this project illustrated in Figure 3-8. Position of the piston was monitored with a Lateral Effect Photodiode (LEPD) Displacement Transducer and Lateral effect driver. The analog command signal was provided by the computer through the DAC. Any difference between the command signal and feedback signal, the error, was used to drive the position of the piston into close correspondence with the required position.
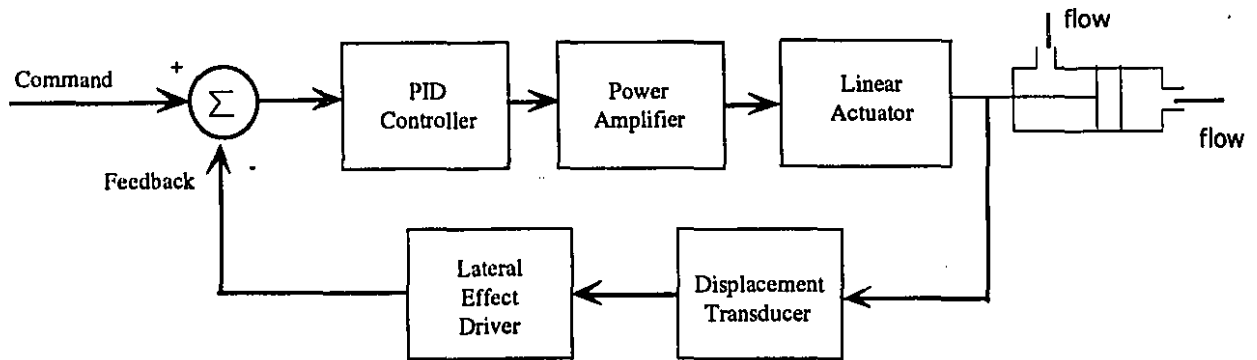
Figure 3-8: Pump feedback control system

i. Linear Actuator

A linear motor (re-cycled from a disk drive) was employed as the actuator. Unfortunately, technical specifications for this device were not available, nor could they be obtained, since the motor does not carry any label stating manufacturer and/or model number. Its dynamic behavior thus had to be characterized by our own measurements.

ii. PID Controller

The PID controller implements the control law:

$$V_0 = K_G e + K_D \frac{de}{dt} + K_I \int e \cdot dt \qquad\qquad 3.4$$

where Kg = gain constant

       Kd = derivative factor

       Ki = integration factor

       e = input error voltage

An electronic circuit (Figure 3-9) was used to implement this controller function. The parameters Kg, Ki, and Kd were adjusted by applying a square wave as command and making the feedback signal correspond with it.

PID Controller
Ian Hunter, Serge Lafontaine and Colin Brenan
21 May 1992
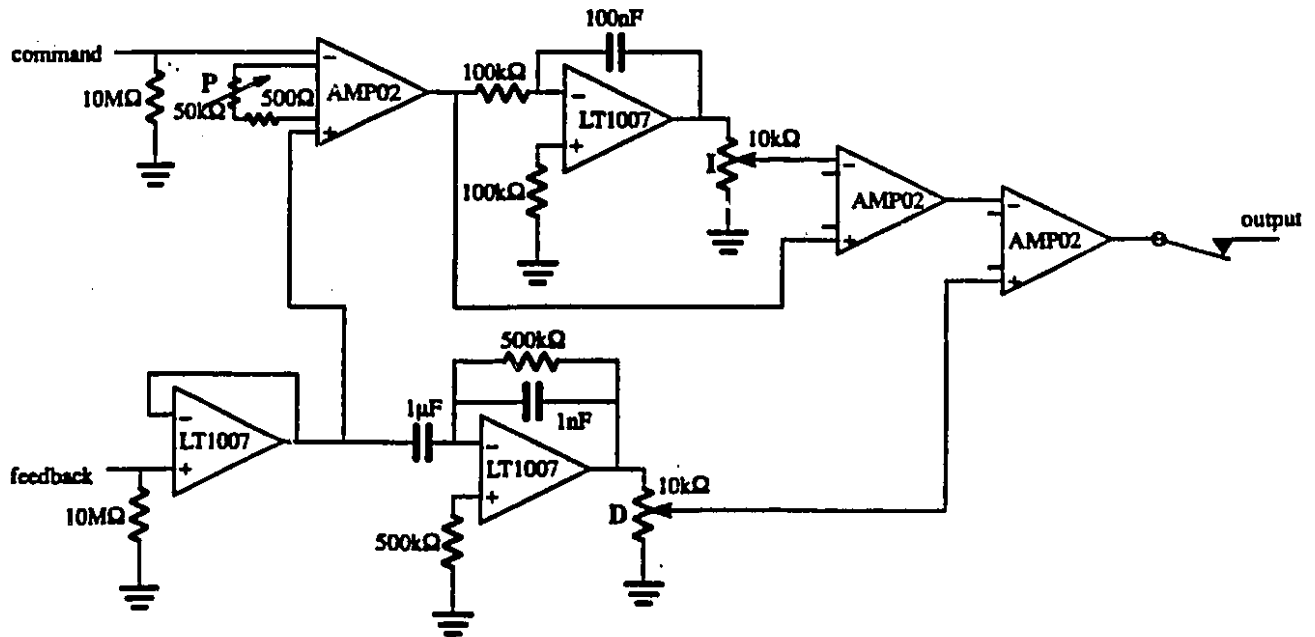
Figure 3-9: The block diagram of a PID analog controller

iii. Power Amplifier

The purpose of the power amplifier was to produce the power necessary to drive the linear motor; i.e. implement the voltage to current conversion needed to drive the inductive load. An integrated power amplifier PA03 was used. Under safe operating conditions, an output span of ± 75V and a current limit of ± 30A are possible, yielding a power rating of 2250W DC or 1125 W for harmonic signals.

The amplifier and its power supply are shown in Figure 3-10. An unregulated power supply was used to maximize efficiency.
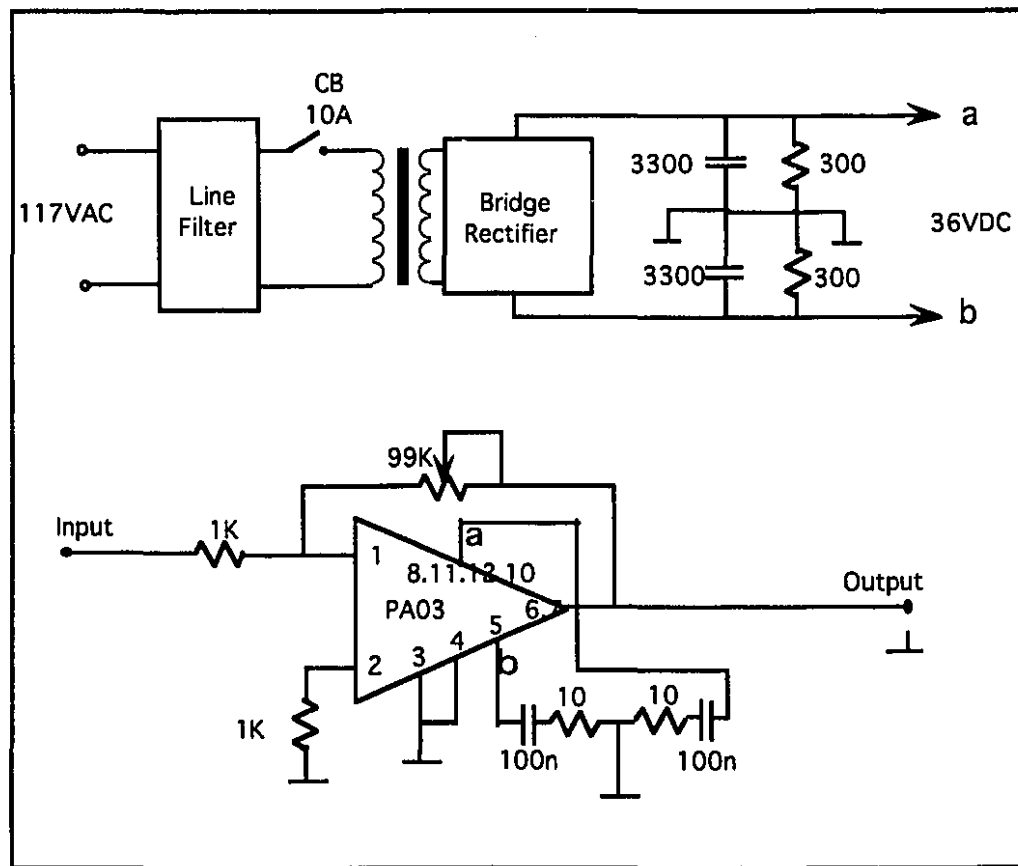
Figure 3-10: Power supply and power amplifier

iv. Lateral Effect Photodiode(LEPD) Displacement Transducer
and Lateral Effect Driver

This transducer involves an optical sensor. Voltage output is linearly proportional to the position of the center of the light spot (Figure 3-11). An electronic realization is shown in Figure 3-12. It was designed and built by Dr. Ian Hunter (Dept. of Biomedical Engineering, McGill University, Montreal, Quebec).
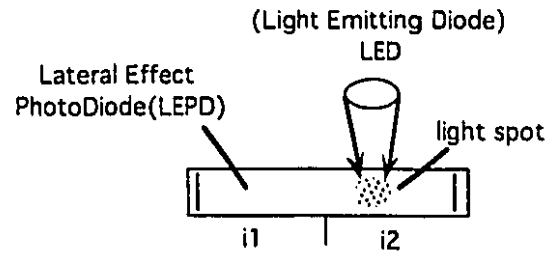
Figure 3-11: Lateral effect photodiode displacement transducer

$$V \propto \frac{i_1 - i_2}{i_1 + i_2} \propto \text{the position of century of light spot}$$
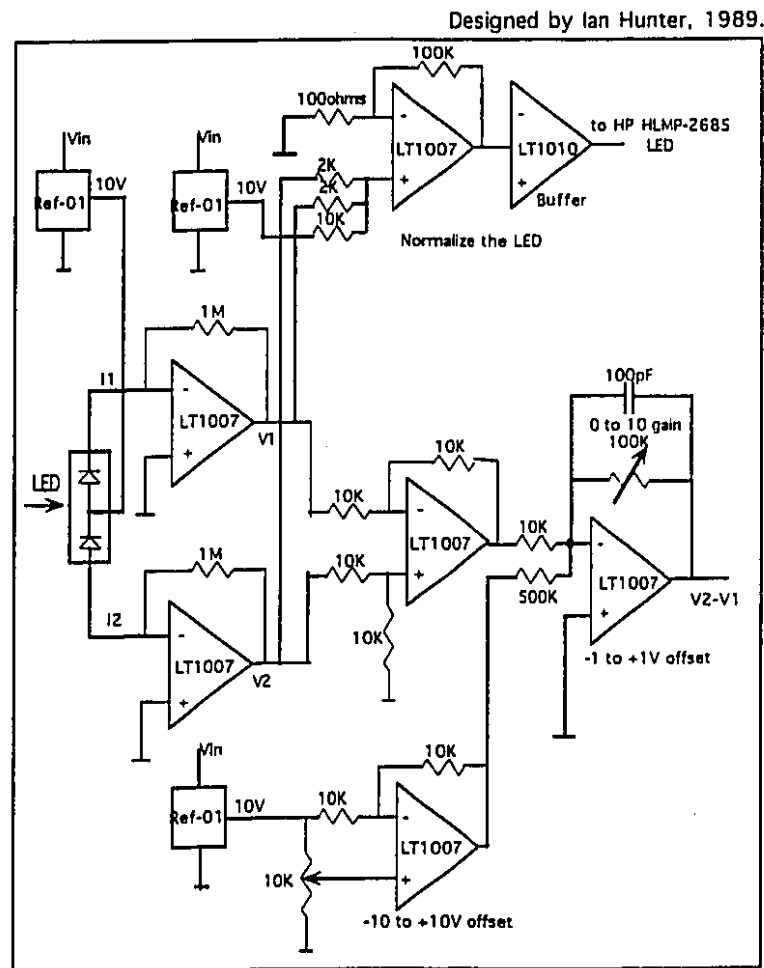
Figure 3-12: Lateral effect photodiode module

v. Pump System Dynamic Properties

The motor's dynamic behavior was tested using a HP3562 DYNAMIC SIGNAL ANALYZER. A set of sinusoidal waves with different frequencies were applied as the command signal. The frequency response was determined from the ratio of the Fourier transform of the measured position signal "feedback" to the Fourier transform of the input signal "command" as

$$H(f) = \frac{F\{x(t)\}}{F\{x_d(t)\}}$$ 3.5

where the script F indicates the Fourier transfer function and x(t) and x_d(t) are the actual and desired piston position signals respectively. H(f) is the transfer function of the pump system. For an ideal system the transfer function should have unity magnitude so that the output perfectly matches the input. Figure 3-13 shows the measured frequency response. It can be seen that the magnitude frequency response was flat to 4 Hz. This means that when using a random volume stimuli to identify bladder hydrodynamics, the frequency range containing high energy from 0 to 4 Hz was possible.
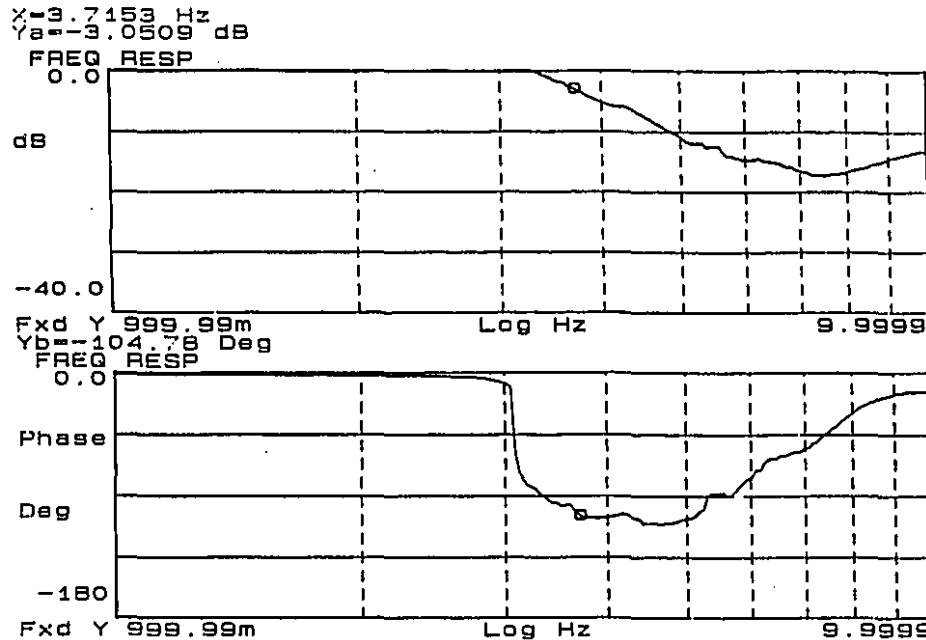
Figure 3-13: Pump's frequency response function

3.3. Software

Data acquisition and experimental control were implemented using NOTEBOOK which works with a variety of METRABYTE data acquisition and control boards [LABTECH, 1991]. It implements real-time data acquisition, real-time process control, real-time graphic display of data and is an easy-to-use icon driven software. Details of the application of this software are listed in Appendix III.

Data analysis was carried out using MATLAB, a technical computing environment for high-performance numeric computation and visualization [Mathworks, 1990]. It integrates numerical analysis, matrix computation, signal processing, and graphics in an easy-to-use environment. Experimental data acquired with NOTEBOOK were transformed to MATLAB for analysis.

4.

Contractile Mechanics of the Urinary Bladder

4.1. Subjects

Six female minipigs, weighing from 25 to 30 kg, were studied. Three had normal bladders while the other three were subjected to bladder outlet obstruction for 10 to 12 weeks.

4.1.1. Obstruction Procedure

The obstruction procedure was carried out at the McGill Animal Resource Center as follows: Each animal was anesthetized with 50 mg/kg animal weight of pentobarbital through an ear vein. The abdomen was opened by a midline suprapubic incision to expose the urinary bladder. A loose uninflated artificial sphincter cuff (size 4.5 cm) was placed around the bladder neck to prevent distending of the posterior urethra lumen during micturition. The incision was closed. The artificial cuff creates a compressive type of obstruction similar to BPH resulting in large residual urine by the 12th to 16th weeks [Guan, Z.C. 1992].

4.1.2. Experimental Procedure

Prior to an experiment, the animal received a pre-anesthetic of Atropine (0.04 mg/Kg animal weight , I.M.), followed by a dose of Ketamine (10 mg/Kg to 20 mg/Kg animal weight , I.M.), and then was maintained on barbiturate anesthesia with Pentobarbital (4-6 mg/Kg animal weight, I.V.) anesthesia until the test was completed. The bladder was surgically exposed through an abdominal incision. Three tubes were inserted into the bladder and sewn to the wall (see Figure 4-1).

to oscillatory pump

to perfusion pump

to pressure transducer
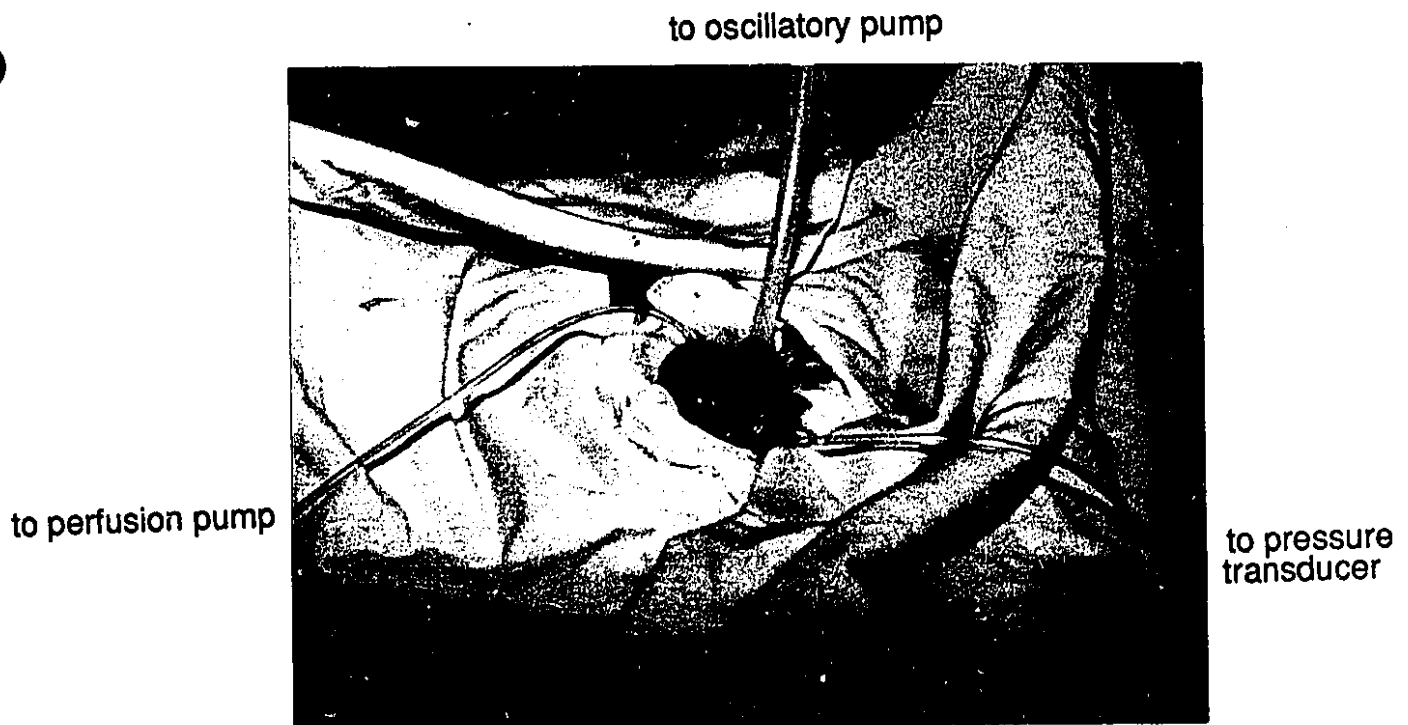
Figure 4-1: The bladder during an experiment

4.2. Apparatus

The three plastic tubes sewn across the bladder wall were connected as follows (see Figure 4-2): (1) a 5.5 mmID, stiff tube was connected to the oscillatory pump whose flow rate was computer controlled to deliver a pseudo-random volume stimulus to the bladder; (2) a 1 mmID tube was connected to the perfusion pump for filling the bladder to various volumes; (3) a 1 mmID tube was connected to a pressure transducer.
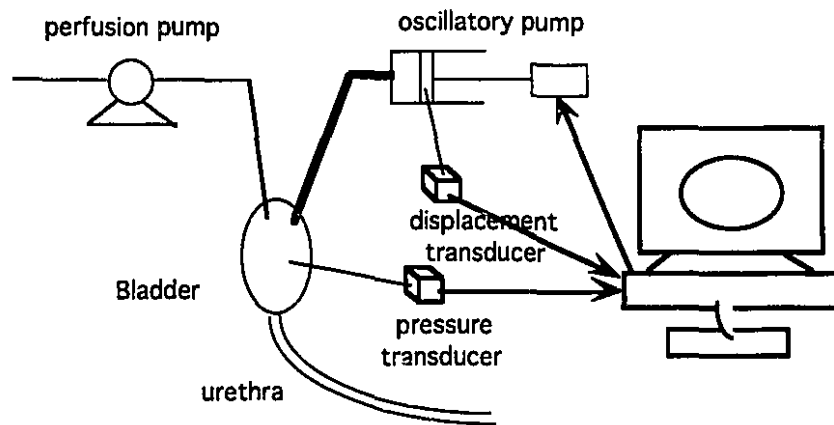
Figure 4-2: Schematic representation of experimental apparatus

4.3. Stimulus

The computer repeatedly generated a 200 point Gaussian white noise signal (GWNS) at a rate of 100Hz on a D/A converter to control the movement of the piston. All experiments were carried out with a peak-to-peak volume amplitude of 5ml. Because of the pump system dynamics, the stimulus actually delivered to the bladder had high power within 4Hz (Figure 4-3).

Perturbation Volume

Power Spectrum of the Volume Stimulus
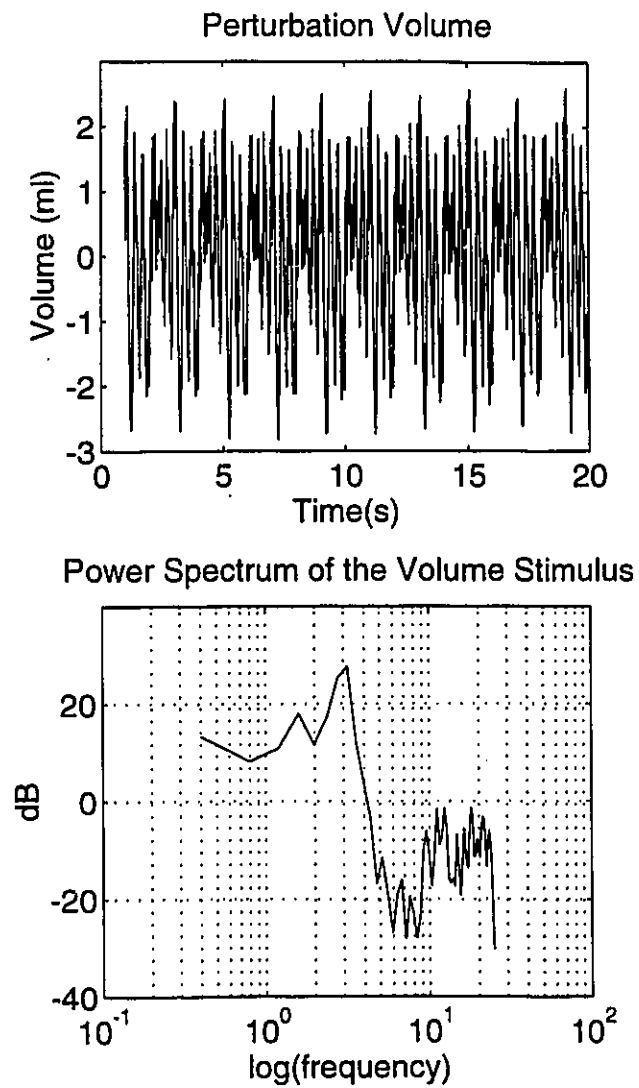
Figure 4-3: Perturbation volume and its power spectrum

4.4. Procedure

Bladder hydrodynamics were assessed at different volumes as follows: Starting with the bladder in an unstrained state, the bladder volume was increased by a fixed amount (20 to 50 ml). After waiting 2 minutes for conditions to stabilize, random volume perturbations were applied for 20 seconds while the perturbation volume and evoked pressure response were recorded by the computer. The procedure was repeated until a volume of 300ml was attained. The procedure was then reversed and the bladder volume gradually returned to the unstrained state.

4.5. Data Acquisition and Processing

Volume and pressure were sampled at 50 Hz by a 12 bit A/D for 20 seconds. The mean detrusor pressure was removed from the pressure signal. Frequency analysis techniques were used to obtain nonparametric estimates of bladder hydrodynamic stiffness in terms of gain, phase and coherence-squared relations between volume and pressure signals. Frequency responses were parameterized by estimating the values of the model:

$$\frac{P}{V} = Is^2 + Bs + K \qquad \qquad 4.1$$

where K = elasticity of the bladder (cmH_2O / cm^3);

         B = viscosity of the bladder ($cmH_2O.s$ / cm^3);

         I = inertia of the bladder($cmH_2O.s^2$ / cm^3)

The hydrodynamic stiffness of this model is

$$Stiffness = G = (K - I\omega^2) + B\omega j \qquad \qquad 4.2$$

which has the real component

$$G_{re} = K - I\omega^2 \qquad\qquad 4.3$$

and the imaginary component

$$G_{im} = B\omega \qquad\qquad 4.4$$

By combining the following equations

$$|G| = \frac{|P|}{|V|}, \qquad G_{re} = |G|\cos(\phi), \qquad G_{im} = |G|\sin(\phi) \qquad\qquad 4.5$$

K can be expressed in terms of the experimentally measured values of

| G | and ϕ and an estimate of I based on bladder wall mass to give

$$K = |G|\cos(\phi) + I\omega^2 \qquad\qquad 4.6$$

Likewise, B can be estimated by

$$B = \frac{|G|\sin(\phi)}{\omega} \qquad\qquad 4.7$$

4.6. Results

4.6.1. Nonparametric Results

Experimental Data

Figure 4-4 shows volume and pressure records for a typical experimental run. It is evident that the pressure changes evoked by the volume perturbation varied symmetrically about the desired tonic level, while the mean pressure changes evoked by the bladder volume change and peak to peak amplitude of the pressure increased with bladder inflation.
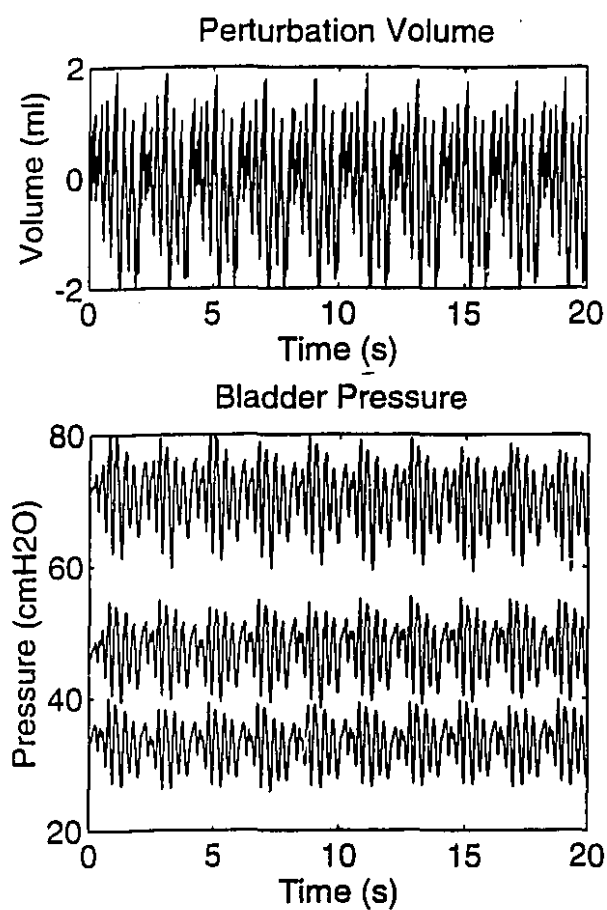
Figure 4-4: Data from a typical experimental run. (upper panel) Transient bladder volume (ml). (lower panel) Transient bladder pressure (cmH_2O) at three different mean values of pressure.

Frequency Response Function

Frequency analysis techniques were used to obtain nonparametric estimates of the bladder hydrodynamic stiffness in terms of gain , phase and coherence-squared relations between volume and bladder pressure (see Figure 4-5). The high values of the coherence squared (>95%) over the full measurement bandwidth (0 to 4 Hz) indicated that the linear, frequency-domain model accounted for most of the observed behavior.

Initial analysis showed that the magnitude increased with frequency as expected but there was an unexpected decrease in phase. The explanation for this was that the volume was estimated by multiplying the displacement of the piston by a calibrating constant. The cylinder was connected to the bladder through a 15 cm long tube which can be expected to lead to a time delay between the piston's position signal and the volume change actually applied to the bladder. We estimated this delay to be 60ms and so shifted the volume signal back 3 points and re-calculated the frequency response function again. Following this correcting procedure, phase estimates did not decrease with frequency anymore (see Figure 4-6).
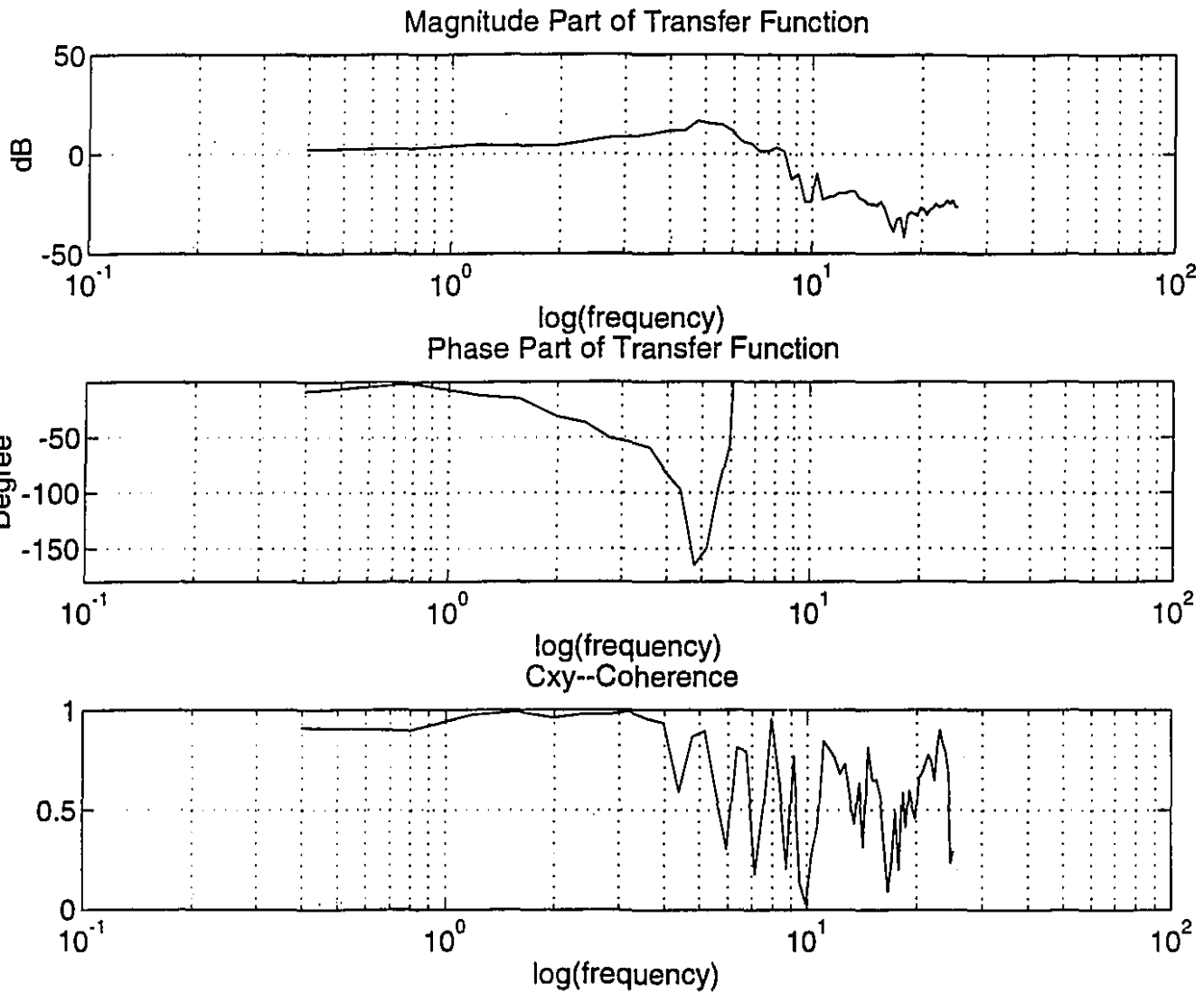
Figure 4-5: Frequency analysis of the raw data shown in Figure 4-4. (top) Hydrodynamic stiffness gain in dB cmH_2O / ml^3. (mid) Phase in degree. (bottom) Coherence-squared.

Magnitude Part of Transfer Function

Phase Part of Transfer Function
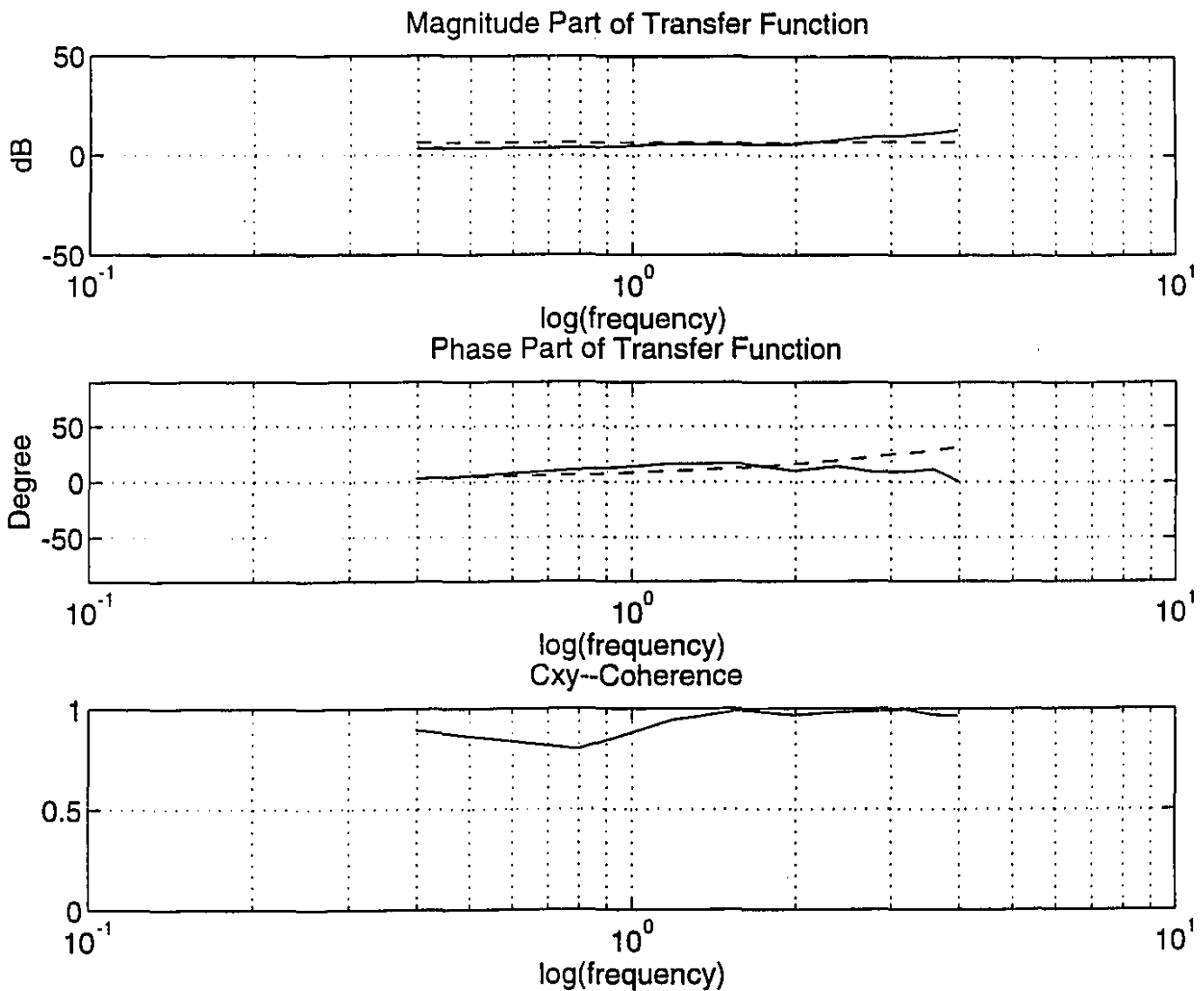
Cxy--Coherence

Figure 4-6: Frequency analysis of the corrected data. (top) Hydrodynamic stiffness gain in dB cmH_2O / ml^3. (mid) Phase in degree. (bottom) Coherence-squared. The gain and phase of the second-order model fitted to the data in the frequency domain are also shown (dash curves) in (top) and (mid).

Stiffness Gain Changes With Volume

Figure 4-7 shows hydrodynamic stiffness gains obtained at six different bladder volumes. It is clear that the low frequency gain increased with bladder inflation.

Magnitude Part of Transfer Function
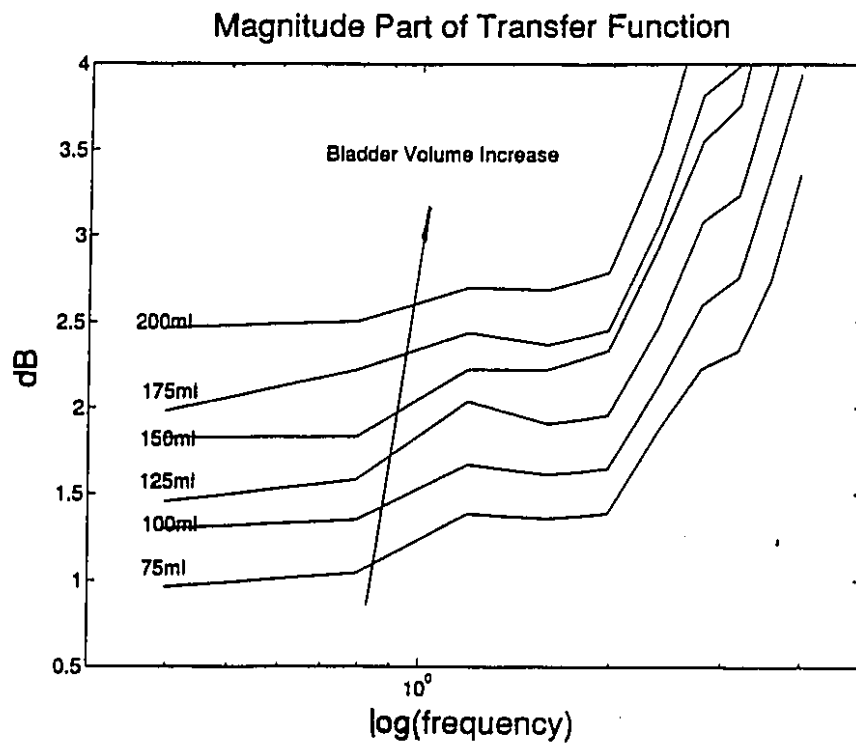
Figure 4-7: Bladder stiffness gains from a normal animal at six different bladder volumes.

4.6.2. Parametric Results

Because the input frequency band was limited to less than 4 Hz (see Figure 4-3), frequency analysis does not give very clear information about the model's structure. However, a model structure may be selected using a priori knowledge about the dynamics of the components of the system and their interactions.

A second order model having inertial (I), viscous (B), and elastic (K) terms was fitted to the hydrodynamic transfer functions. Figure 4-6 shows a nonparametric frequency response function superimposed on the corresponding second-order system's frequency response function. Parameter values were estimated by using the equations described in Section 4.5. The similarity of the two curves demonstrated that the parametric model (Equation 4.1) provides an adequate description of the experimental data obtained for a particular set of operating conditions. Even through the fit is not perfect, the simplicity of the model and the physical interpretation of its elements makes it useful.

The estimated model parameters K and B increased approximately in proportion to the bladder volume. This made it possible to use linear regression techniques to estimate the straight line approximation to the data points for each subject. Note that since the bladder size was different in each animal, volume was normalized as strain ε using the relation

$$\varepsilon = \sqrt[3]{\frac{V}{V_0}} - 1 \qquad\qquad 4.8$$

Figure 4-8 shows the estimated model parameters K (*) and B (*) as functions of strain and their regression lines for one animal. The correlation coefficient r conveys how good these fits are. The slopes of

K and B vs. ε represent how rapidly the elastic constant and viscous constants increase with the bladder inflation. It is expected that they will be quite different between normal bladders and obstructed ones.

Elastic Parameters for a Normal Bladder

$$K = 4.0 * strain + 1.1$$
$$r = 0.91$$

Viscous Parameters for a Normal Bladder

$$B = 0.14 * strain + 0.02$$
$$r = 0.81$$

Figure 4-8: (upper panel) The elastic parameter (K) plotted as a function of the strain (ε) for a subject and the regression line fitted to the relation between K and ε . (lower panel) The viscous parameter (B) plotted as a function of the strain (ε) for a subject and the regression line fitted to the relation between B and ε.

4.6.3. Obstructed Animals

The same experimental procedure and data processing methods were applied to an obstructed bladder. The frequency analysis of a pair of volume/pressure signals is shown in Figure 4-9. The gain and phase of the second-order model fitted to this frequency properties were superimposed on the nonparametric values. Clearly, the second-order model closely approximates the obstructed bladder behavior. The high value of the coherence-squared indicated that the linear, dynamic relation between volume and pressure described by the gain and phase curves accounts for most of the output.

The hydrodynamic stiffness changed systematically as a function of the bladder volume. This is illustrated in Figure 4-10, which showed stiffness gain curves obtained at six different levels of the bladder volume for an obstructed bladder. As with the normal animals, the low frequency gain increased with increasing levels of bladder volume. But, the increase of the gain was more rapid in the obstructed than in the normal bladder.

The estimated model parameters also varied systematically with the bladder volume as illustrated for an obstructed bladder in Figures 4-11. The elastic parameter (K) increased approximately in proportion to the bladder volume.
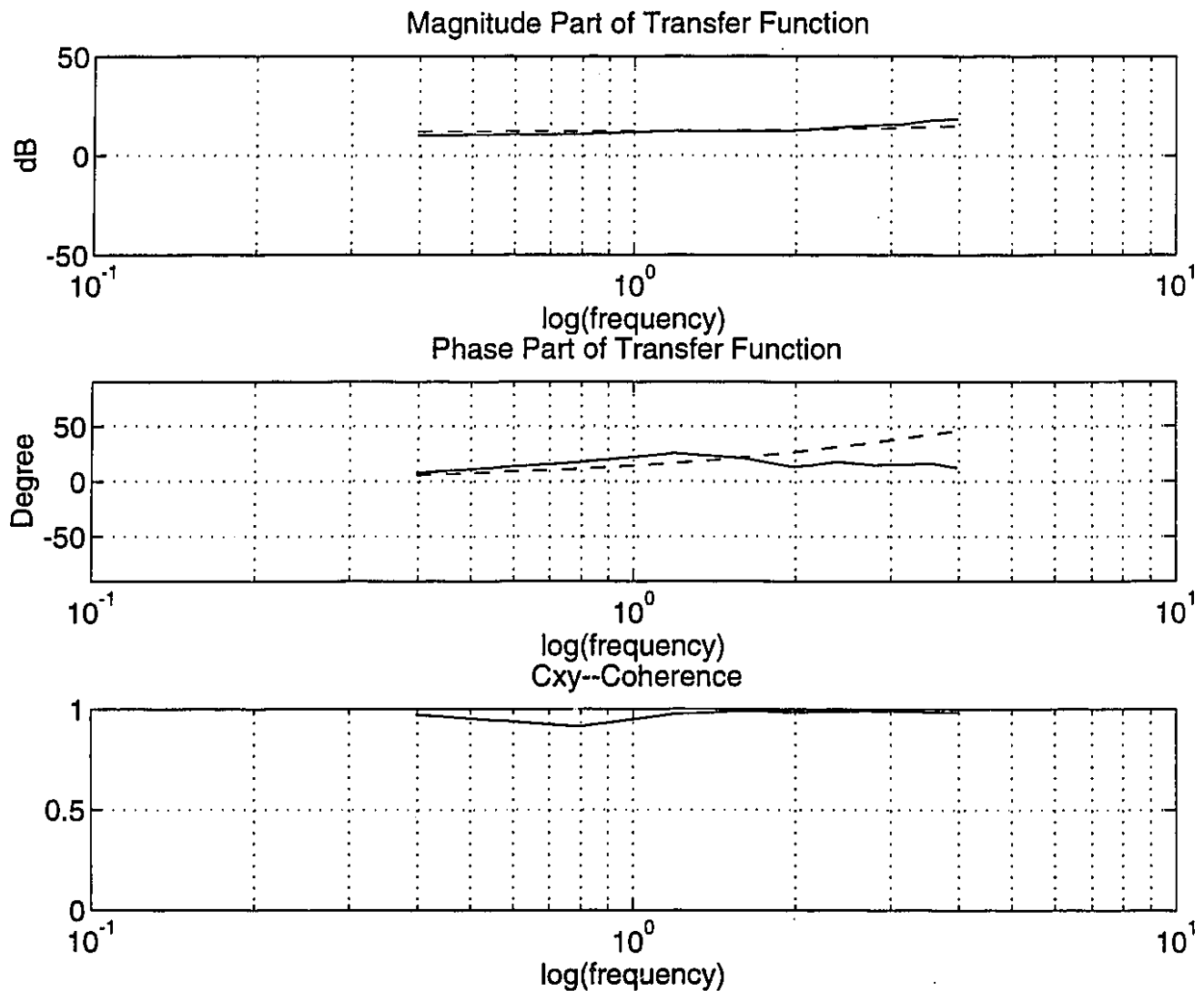
Figure 4-9: Frequency analysis of the corrected data from an obstructed animal. (top) Stiffness gain in dB cmH_2O / ml^3. (mid) Phase in degree. (bottom) Coherence-squared. The gain and phase of the second-order model fitted to the data in the frequency domain are also shown (dash curves) in (top) and (mid).

Magnitude Part of Transfer Function
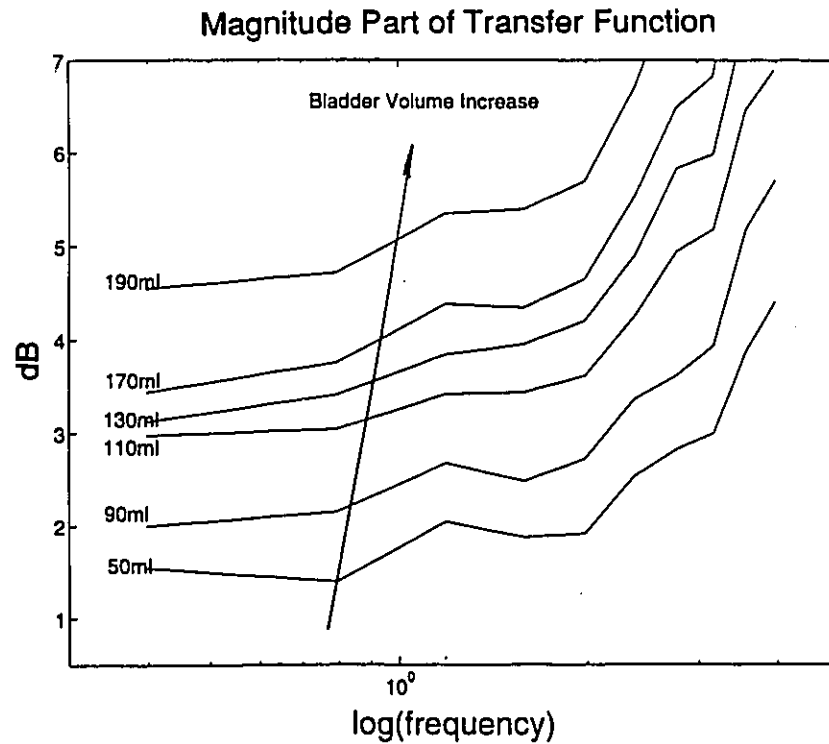
Figure 4-10: Bladder stiffness gains from an obstructed animal at six different bladder volumes. The gain increased more rapidly with volume than that of the normal bladder shown in Figure 4-7.

Elastic Parameters for an Obstructed Bladder

K=5.6*strain+2.3
r=0.73

Viscous Parameters for an Obstructed Bladder

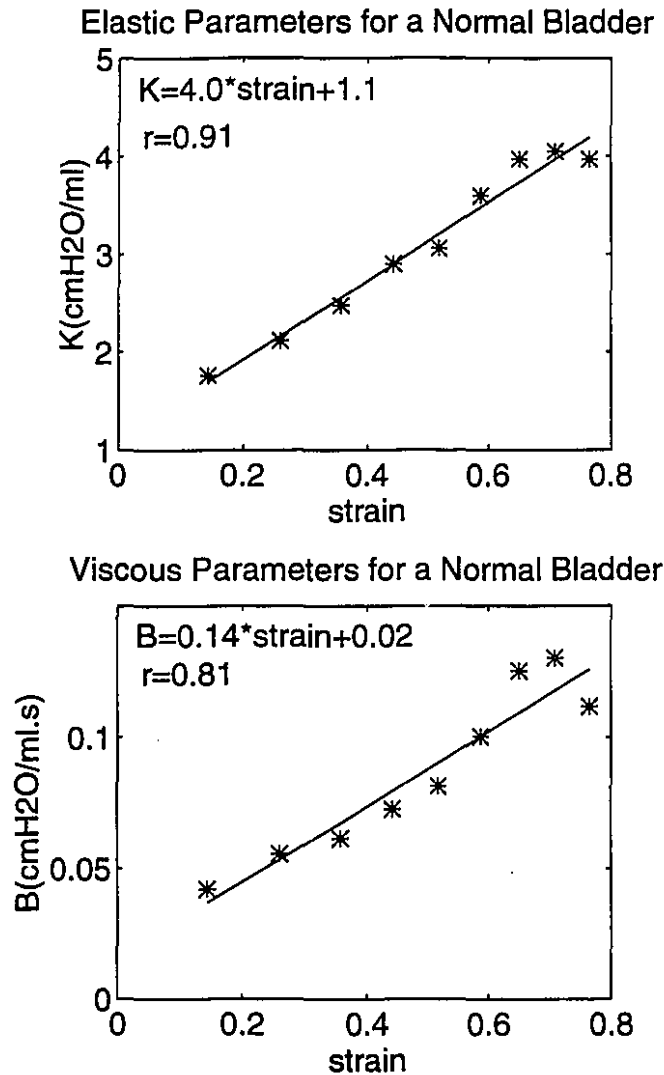B=0.15*strain+0.12
r=0.57
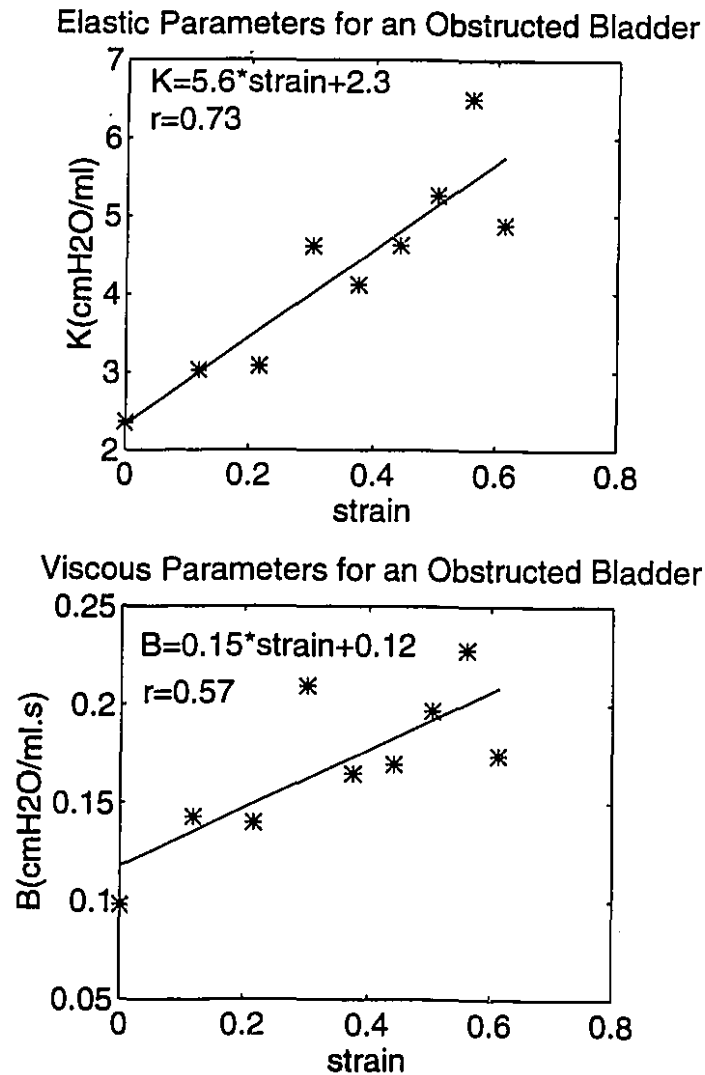
Figure 4-11: (upper panel) The elastic parameter (K) plotted as a function of the strain (ε) for a subject and the regression line fitted to the relation between K and ε. (lower panel) The viscous parameter (B) plotted as a function of the strain (ε) for a subject and the regression line fitted to the relation between B and ε

4.6.4. Summary Results

The elastic parameter K was selected as the basis for distinguishing between normal and obstructed animals. The results from six animals are collected in Table 4-1 and presented visually in Figure 4-12. **Slopes** of K vs. strain in the cases of bladder inflation and deflation and their average value are shown respectively, as are the correlation coefficients (r). Lower slopes were obvious in the normal group compared to the obstructed group. Thus, bladder stiffness increased less rapidly with volume in normal animals than in those which had been obstructed. For most experiments, the values of the correlation coefficient in the cases of the bladder inflation are higher than those in the cases of the bladder deflation.

Table 4-1 The result of linear regression analysis - Slope of elastic parameter (K) for each subject.

Pig Group	Ascending		Descending		Average	
	Slope	r	Slope	r	Slope	r
Normal I	0.8	0.69	X*	X*	0.80	0.69
II	2.8	0.74	1.46	0.70	1.77	0.72
III	0.7	0.54	0.61	0.60	0.65	0.57
Obstructed I	5.6	0.73	4.6	0.55	5.08	0.64
II	4.3	0.61	3.9	0.48	4.13	0.55
III	2.9	0.84	1.4	0.45	2.42	0.65

* X is an incomplete datum.
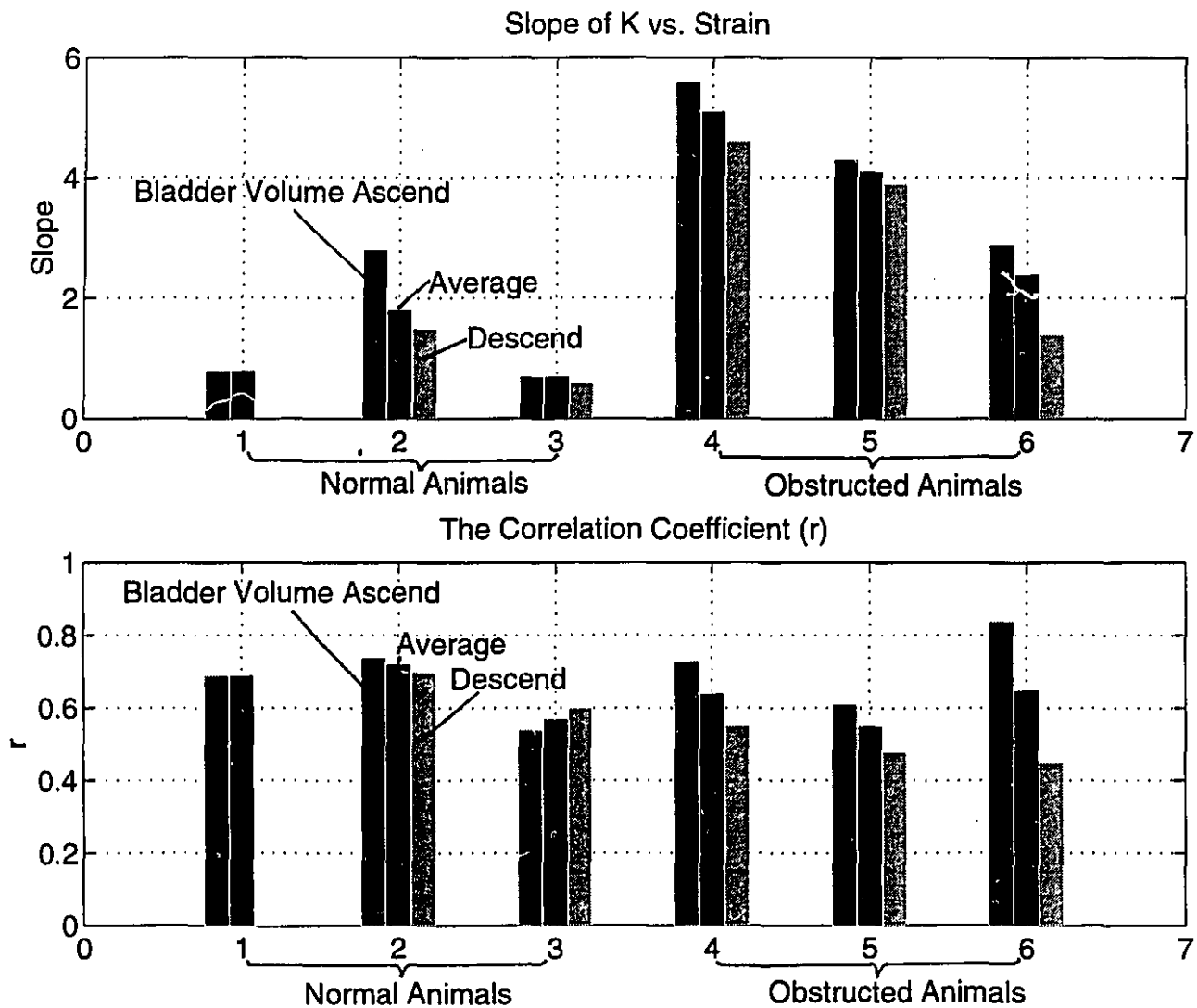
Figure 4-12: Visual presentation of the result of linear regression analysis. (upper panel) The slopes of K vs. ε in the cases of bladder inflation and deflation and their average value. (lower panel) Respective correlation coefficients (r).

4.7. Discussion

The major finding in this study was that the elasticity of the bladder increases nearly linearly with volume increases in both normal and obstructed animals. However, the rate of increase was substantially greater in the obstructed animals than in the normals. A possible explanation of this is that the collagen content was significantly increased in the obstruction group, i.e. the fibrotic degeneration had occurred. This could cause the difference of the elastic constant between the different groups.

An important methodological issue in interpreting these data is the possible effects of anesthesia on bladder mechanical properties. In Chapter 2 we mentioned that the force developed by muscle depends on two mechanisms: contractile mechanics and activation dynamics. When we focus on contractile mechanics, we hope to minimize the effect of activation dynamics. During the experiment, animals received anesthesia (Atropine, Ketamine, Pentobarbital) which depresses the CNS, depresses the activity of smooth muscle of the urethra and urinary bladder, keeps bladder in relax situation. It is consistent with our experimental conditions which assumes the level of neural activation remains constant.

Previous investigations of bladder contractile mechanics were carried out by filling the bladder slowly and measuring the pressure produced. This yields a pseudostatic pressure-volume relationship called cystometry which reflects only the bladder's elastic properties at rest. Mastrigt et al. (1978) developed a 14-parameter model to describe bladder muscle's passive properties and used stepwise volume stimuli and pressure responses to fit 8 parameters in the model. Although

individual model elements were given a meaning related to muscle function, the model's complexity prevented its widespread application. We measured hydrodynamic stiffness with short experimental records by applying a stochastic volume stimulus at a constant bladder volume and parameterized nonparametric hydrodynamic stiffness transfer function with a second-order lumped parameter model. The major advantage of modeling bladder hydrodynamics with Equation 4.1 is that each parameter has a straightforward interpretation in terms of the underlying physics (e.g. inertia, viscosity, elasticity). By repeating the identification procedure as the bladder is filled and emptied, we monitored how the bladder mechanics (model parameters) changed with bladder volume. Comparison of the results of experiments performed before and after obstruction provided quantitative descriptions of the effects of obstruction on bladder mechanics. This approach shows promise for distinguishing normal and obstructed bladder mechanics.

We estimated bladder hydrodynamics by using stochastic volume perturbations at bladder volume over a range which did not reach the elastic limit (Pdet < 70 cmH2O), since higher pressures were found to cause leakage. The elastic stiffness, K, was found to increase nearly linearly as a function of the bladder volume as illustrated in Figure 4-13. The values of K in the ascending phase of the experiment were always larger than the values in the descending phase. This may be due to the plasticity of the bladder muscle. The rest length of the bladder muscle tends to increase when the muscle is stretched passively, especially if a high passive force is developed [Coolsaet et al., 1976; Van Mastrigt et al.,1978].
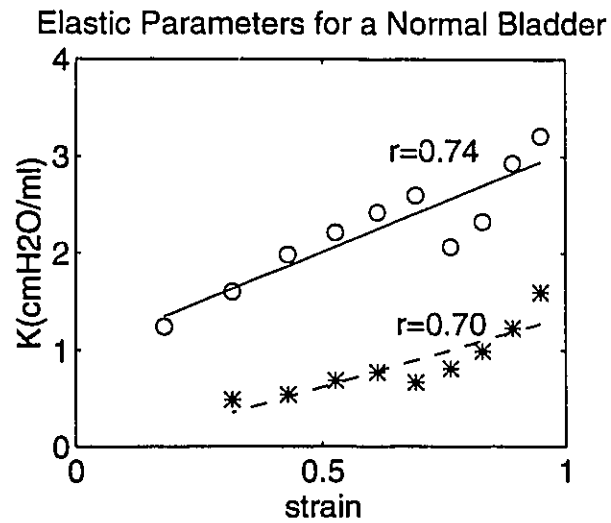
Figure 4-13: Plots of K vs. ε for bladder volume ascending "o" and descending "*" experiments for one subject and the regression lines (K = 2.08 × ε + 0.98) for '——' ; (K = 1.46 × ε - 0.1) for '---' fitted to the original data.

5.

Conclusion

5.1. Summary

The objective of this thesis was to investigate bladder hydrodynamics using a system identification approach and to provide a quantitative description of the effects of obstruction on the bladder mechanics.

Our strategy was to apply a stochastic volume stimulus, measure the evoked pressure changes, to determine bladder hydrodynamic stiffness at a particular bladder volume by analyzing a pair of volume-pressure data, and then to parameterize the frequency response data by estimating the model parameters (Equation 4.1). By repeating the identification procedure as the bladder was filled and emptied, we monitored how the bladder mechanics (model parameters) changes with bladder volume. Comparison of the results of experiments performed before and after obstruction provided quantitative descriptions of the effects of obstruction on bladder mechanics.

We designed and built an experimental apparatus and developed an experimental paradigm for nonparametric and parametric identification of bladder hydrodynamics.

The results demonstrate that a second-order lumped parameter model provide a reasonable quantitative description of bladder hydrodynamics at constant volume. Model parameters change with volume; the elastic parameter increase approximate linearly with volume in both normal and obstructed animals. The rate of increase was substantially greater in obstructed animals than in normal animals. Consequently, this approach shows promise for distinguishing normal and obstructed bladder mechanics.

5.2. Recommendations

The identification approach used here has been proven to be quite successful and it is recommended that the work be extended. In the continuation of the work the following aspects are worthy of investigation:

(i). Develop a more precise volume measurement tool. In our current experimental system, the volume of perturbing water introduced into the bladder was estimated by multiplying the position of the piston by a calibrating constant. This method of volume measurement entails a time delay comparing with the actual volume signal and a magnitude error caused by the presence of air bubbles in the tube and/or in the cylinder. A more precise way would be to place a flow transducer probe adjacent to the bladder. This would measure the flow actually delivered to the bladder. Volume could then be obtained by numerical integration of the flow signal.

(ii). It would also be useful to apply a higher oscillatory frequency. It is known that the low speed of activation and contraction of the detrusor permitted the use of frequencies lower than those required in

the fast-activating striated muscle. However, there is no indication in the literature of the boundary value of the frequency that the detrusor muscle can respond to. We obtained the bladder hydrodynamic stiffness over a very limited frequency band which did not give us very clear information about the structure of the bladder muscle system. We therefore had to depend on a priori knowledge. Increased stimulus bandwidth would require on improved pump system.

(iii). Increase the number of the animals in both groups and unify the experimental conditions. The number of animals in this study was limited and the operation procedure and experiment paradigm were improved with each experiment. As a result these data are limited and the significance of our results is somewhat uncertain. Much work remains to be done to obtain more reliable results on the effects of obstruction on contractile mechanics of bladder muscle.

(iv). Combining our random volume stimulus with an urethral perfusion stimulus would permit an investigation of how bladder hydrodynamic stiffness changes with the level of activation. This would provide a description of the effects of obstruction on activation dynamics of bladder muscle.

(v). The technique could also be used to evaluate the effectiveness of a trial drug or prostatectomy to bladder muscle mechanical properties. This could provide information about the underlying pathology of BPH. This method can only be used in animal study.

APPENDIX I

SPECIFICATIONS AT 25°C (77°F)

pounds/inch²

@ STANDARD V_s = 9 VDC.	PRESSURE RANGE (Custom Ranges Available)									
PARAMETER	±1, ±5 PSID			0-1, 0-5, 0-15 PSID			0-1 PSIG, 0-5, 0-15			**UNITS**
	MIN	TYP	MAX	MIN	TYP	MAX	MIN	TYP	MAX	
FULL SCALE OUTPUT (POS PRESS.)	5.9	5.92-6.08	6.1	5.9	5.92-6.08	6.1	5.9	5.92-6.08	6.1	VDC
NULL OFFSET	3.9	3.92-4.08	4.1	1.9	1.92-2.08	2.1	1.9	1.92-2.08	2.1	VDC
SPAN*	1.8	1.84-2.16	2.2	3.8	3.84-4.16	4.2	3.8	3.84-4.16	4.2	VDC
LINEARITY (BEST FIT)		±0.3	±0.5		±0.3	±0.5		±0.3	±0.5	%SPAN
HYSTERESIS		±0.003	±0.01		±0.003	±0.01		±0.003	±0.01	%SPAN
REPEATABILITY		±0.005	±0.05		±0.005	±0.05		±0.005	±0.05	%SPAN
TEMPERATURE ERROR NULL −30° to +100°C SPAN −30° to +100°C		±1.6 ±1.0	±3.0 ±1.5		±1.6 ±1.0	±3.0 ±1.5		±1.6 ±1.0	±3.0 ±1.5	%SPAN %SPAN
STABILITY (1 year)		±1.0			±1.0			±1.0		%SPAN
SUPPLY VOLTAGE (V_s)**	7.5	9	15	7.5	9	15	7.5	9	15	VDC
SUPPLY CURRENT (QUIESCENT) 10K Load		8	15		8	15		8	15	MA
EMI CHANGE IN OUTPUT DUE TO RF FIELD OF 200V/M. 10KHz to 1GHz (BY SPECIAL ORDER)		±0.2	±1.0		±0.2	±1.0		±.02	±1.0	VDC
TRANSIENT VOLTAGE ON V_s			50			50			50	V/1 MSEC
COMMON MODE PRESSURE			15			15				PSI
PRESSURE OVERLOAD (POS PRESS.)*** (NEG PRESS.)			20X 2X			10X 1X			10X	RATED PRESSURE
BURST PRESSURE (POS PRESS.)*** (NEG PRESS.)			50X 2X			10X 1X			10X	RATED PRESSURE

*Span is the Algebraic Difference Between End Points (Null Offset and Full Scale Output)
DC V_s Available by Special Order, Contact Kavico
RATING SUBJECT TO USERS MOUNTING DESIGN

$V_S = 12\,V$ CONVENIENT

OPERATION DATA

Electrical Output	Load Current 2MA Maximum
	Output impedance less than 100 ohms
	10 MV RMS Ripple Max
	Short circuit protected
	Common lead is grounded to case
	Response time 15 MSEC @ 63% Full Scale step pressure based on min port ID of .125 in.
Media Compatibility	96% Alumina ceramic. Seal material and users input port materials. Low pressure or reference pressure ports on differential models require dry gas or air, or vacuum for maximum stability.
Operating Life	Within design specifications after 10 million Full Scale cycles
Volumetric Displacement	Less than 0.001 cu. in.
Weight	43 GRMS (1.5 oz)
Termination	3 .01 x .025 in. pins or 3 22 awg leads 12 in. length
Mounting	Circumferential compression by users design
Vacuum Measurements	Vacuum may be applied to gage units within 100% of Full Scale positive pressure. Select null offset for bidirectional outputs.
Environmental	Designed to withstand the following based on suitable mounting design
	10G 10-2000 Hz Vibration
	50G 1/2 sine shock
	Humidity MIL-STD-202 method 106 10 day cycling temperature

CHARACTERISTICS

BIDIRECTIONAL PRESSURE % FULL SCALE

Increasing or decreasing supply voltage V_s from 9v standard calibration $= \frac{V_s}{9} \times$ calibrated output

UNIDIRECTIONAL PRESSURE % FULL SCALE
TYPICAL OUTPUT CHARACTERISTICS
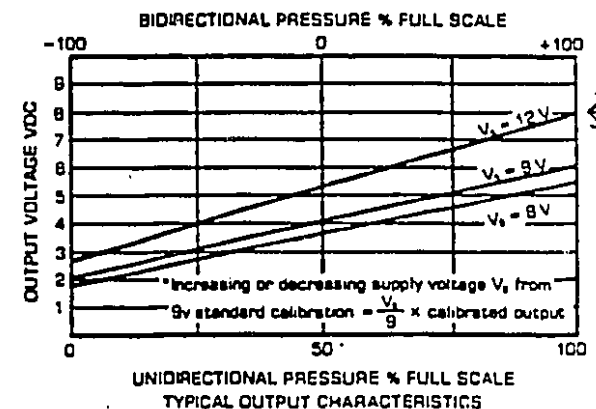
HOW TO ORDER

P612 — 5 — A — A — 1 — A

PRESSURE RANGE	
0-1 PSIG	1
0-5 PSI	5
0-15 PSI	15
±1 PSID	2
±5 PSID	10
±15 PSID	16

REFERENCE	
ABSOLUTE	A
GAGE	G
DIFFERENTIAL	D

SEAL MATERIAL	
SILICONE	A
FLUOROSILICONE	E

TERMINATION	
12 in leads	1
3 Pins	2

ELECTRICAL
STANDARD   A

SEAL ORDER GUIDE

Type	Input Port Seal Material	Input Media Compatibility**	Maximum Seal Temperature Range °C
A	Silicone	Organic liquids, alcohols, ammonia gas	−54°C to +232°C
E	Fluorosilicone	solvents, oils, fuels	−73°C to +177°C

APPENDIX II

FEATURES

- Cutoff Frequencies (f_C) from 0.1Hz to 50kHz
- Large Tuning Ratio - to 500:1
- High Performance:
  - Input Impedance - $10^9\Omega$
  - Stability of f_C - 0.05%/°C
  - Output Noise Voltage - 75μV RMS
  - Output Impedance - 1Ω

APPLICATIONS

- Anti-Aliasing
- Vibration Studies
- Noise Reduction
- Band Isolation

DESCRIPTION

Frequency Devices, Inc. offers this family of resistive tuneable two, four, and six-pole lowpass active filters in both Butterworth and Bessel configurations. The pass band of each device extends from dc, where a non-inverting gain is held within 0.02dB of unity, to the selected cutoff frequency, f_C. The dc offset voltage may be externally adjusted to zero. Offset drift is less than 30μV/°C for the two and four-pole devices and less than 75 V/°C for the six-pole devices. The cutoff frequency adjustment range of any particular unit is 200:1 or 500:1. Table 1 below defines this range for each filter.

BUTTERWORTH			BESSEL			TUNING RANGE (Hz)	
2-Pole	4-Pole	6-Pole	2-Pole	4-Pole	6-Pole	f_{cmin}	f_{cmax}
738BT-1	730BT-1	736BT-1	738LT-1	730LT-1	736LT-1	0.1	20
738BT-2	730BT-2	736BT-2	738LT-2	730LT-2	736LT-2	1	200
738BT-3	730BT-3	736BT-3	738LT-3	730LT-3	736LT-3	10	2K
738BT-4	730BT-4	736BT-4	738LT-4	730LT-4	736LT-4	100	20K
748BT-1	740BT-1	746BT-1	748LT-1	740LT-1	746LT-1	0.5	50
748BT-2	740BT-2	746BT-2	748LT-2	740LT-2	746LT-2	1	500
748BT-3	740BT-3	746BT-3	748LT-3	740LT-3	746LT-3	10	.5K
748BT-4	740BT-4	746BT-4	748LT-4	740LT-4	746LT-4	100	50K

TABLE 1: Cutoff Frequency Adjustment Range from f_{cmin} to f_{cmax}

FREQUENCY RESPONSE

STEP RESPONSE
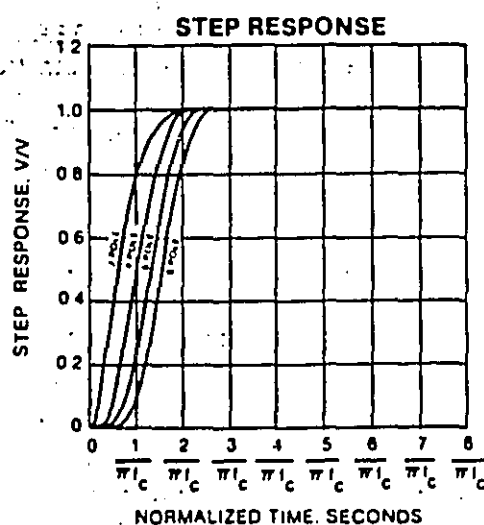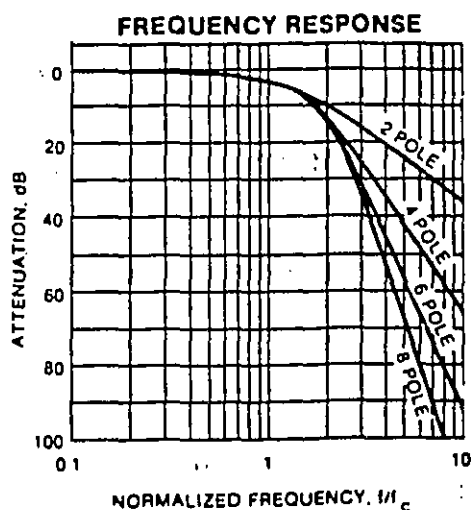
NORMALIZED FREQUENCY RESPONSE TABLE

f/f_c	2 POLE		4 POLE		6 POLE		8 POLE	
	A(dB)	$\psi(°)$	A(dB)	$\psi(°)$	A(dB)	$\psi(°)$	A(dB)	$\psi(°)$
0.00	0.00	0.0	0.00	0.0	0.00	0.0	0.00	0.0
0.10	0.03	-7.8	0.03	-12.1	0.03	-15.5	0.03	-18.2
0.20	0.11	-15.6	0.11	-24.2	0.12	-31.0	0.12	-36.4
0.30	0.25	-23.4	0.25	-36.3	0.26	-46.5	0.26	-54.7
0.40	0.45	-31.2	0.45	-48.4	0.46	-62.0	0.47	-72.9
0.50	0.71	-38.3	0.71	-60.6	0.73	-77.4	0.74	-91.1
0.60	1.04	-46.4	1.02	-72.7	1.05	-92.9	1.06	-109.3
0.65	1.24	-50.1	1.21	-78.7	1.24	-100.7	1.25	-118.4
0.70	1.44	-53.8	1.41	-84.8	1.44	-108.4	1.45	-127.5
0.75	1.67	-57.4	1.63	-90.8	1.66	-116.2	1.67	-136.6
0.80	1.91	-61.0	1.86	-96.8	1.89	-123.9	1.91	-145.7
0.85	2.16	-64.4	2.12	-102.9	2.15	-131.7	2.16	-154.9
0.90	2.43	-67.8	2.40	-108.9	2.42	-139.4	2.42	-164.0
0.95	2.72	-71.1	2.69	-114.9	2.70	-147.1	2.71	-173.1
1.00	3.01	-74.3	3.01	-120.8	3.01	-154.9	3.01	-182.2
1.10	3.63	-80.4	3.71	-132.6	3.68	-170.4	3.67	-200.4
1.20	4.28	-86.1	4.51	-144.2	4.44	-185.8	4.40	-218.6
1.30	4.96	-91.4	5.39	-155.5	5.29	-201.2	5.20	-236.8
1.40	5.66	-96.3	6.37	-166.4	6.23	-216.5	6.10	-255.0
1.50	6.36	-100.8	7.42	-176.7	7.29	-231.5	7.08	-273.2
2.00	9.82	-118.4	13.41	-219.4	14.17	-300.2	13.68	-361.9
2.50	12.96	-130.1	19.43	-247.8	22.54	-350.7	23.08	-436.4
3.00	15.74	-138.2	25.09	-267.3	30.70	-384.7	33.38	-489.2
3.50	18.19	-144.0	30.04	-281.0	38.08	-408.4	42.85	-525.4
4.00	20.36	-148.5	34.43	-291.2	44.68	-425.8	51.81	-551.8
5.00	24.07	-154.8	41.92	-305.2	55.93	-449.5	66.80	-587.3
6.00	27.15	-159.0	48.12	-314.5	65.25	-465.0	79.22	-610.2
7.00	29.77	-162.0	53.40	-321.1	73.17	-475.9	89.80	-626.3
8.00	32.06	-164.2	57.99	-326.0	80.07	-484.0	98.99	-638.2
9.00	34.08	-166.0	62.05	-329.8	86.16	-490.3	107.12	-647.4
10.00	35.89	-167.4	65.68	-332.8	91.62	-495.3	114.40	-654.8

NOTE: Eight pole not available in Resistive Tuneable configuration at this time. See Fixed Frequency Lowpass Filter data section.

(Typical @ 25°C and ±V_S = 15V unless otherwise noted)

ACTIVE CHARACTERISTICS	TWO-POLE 738/748	FOUR-POLE 730/740	SIX-POLE 736/746
Tolerance of f_c [1]	±3%	±3%	±3%
Stability of f_c	±0.05%/°C [1]	±0.05%/°C [1]	±0.05%/°C [1]
	-- [2]		-- [2]
Input			
Impedance	$10^9 \Omega$	$10^9 \Omega$	$10^9 \Omega$
Voltage Range	±10V	±10V	±10V
Bias Current	10nA	10nA	10nA
Output [3]			
Rate Output @ 2mA	±10V	±10V	±10V
Noise [4]	75µV RMS	75µV RMS	75µV RMS
Resistance	1Ω	1Ω	1Ω
Offset Voltage [5]	±5mV	±5mV	±5mV
Offset Drift	±30µV/°C	±50µV/°C	±75µV/°C
dc Gain (non-inverting)	0±0.02dB	0±0.02dB	0±0.02dB
TEMPERATURE			
Operating	0 to +70°C	0 to +70°C	0 to +70°C
Storage	−25 to +85°C	−25 to +85°C	−25 to +85°C
POWER SUPPLY(DC)			
Rated Voltage	±15V	±15V	±15V
Operating	±12 to ±18V	±12 to ±18V	±12 to ±18V
Quiescent Current	8mA (738)	12mA (730)	16mA (736)
	16mA (748)	22mA (740)	28mA (746)

NOTES:
1) Applicable when using matched 1%, 100ppm/°C resistors.
2) Frequency drifts of 0.01%/°C available on request.
3) Output short circuit protected to ground.
4) Noise, dc to 50kHz, excluding dc offset, input grounded.
5) Adjustable to zero using 1kΩ trim pot. F.D.I. P/N 79PR1K.

APPENDIX III

1. Application of Perturbations From File

When we select Analog Output as the block type in the BLOCK MENU and choose open-loop control function (see Table 6-1), NOTEBOOK transmits the contents of a data file (called a waveform file) to a specified interface channel number on the DAS-16 board and pass through power amplifier to control the motor move. Typical perturbations for the system identification might be sinusoidal oscillation, step function, ramp function, Gaussian white noise, and pseudo-random binary sequences. These wavefiles can be created with MATLAB.

Block Type	Analog Output
Loop	Open
Wavefile File Name	wf.prn
Number of Points to use	200
Sampling Rate,Hz	100
Stage Duration	20

Table 6-1: BLOCK MENU

2. Set Experiment Condition

Data acquisition option can be determined by setting the parameters in ANALOG INPUT ICON MENU (Table 6-2). The scale factor and offset may be used to convert incoming data (voltage) to engineering units (e.g. cmH2O). After calibrating the transducer and using 'polyfit(x,y,n)' in the MATLAB to fit calibration data, we get:

For pressure transducer P1:

Voltage = 0.1005 * Pressure + 0.5852

Engineering Unit = (voltage + offset) * scale

Pressure = (voltage - 0.5852) * 9.9947

Block Type	Analog Input
Block Units	Volts
Interface Device	DAS-16
Interface Channel No.[0..15]	1
Input Range	10V
Scale Factor	10.1971
Offset Constant	0.4997
Sampling Rate,Hz	50
Stage Duration	20

Table 6-2: BLOCK MENU

3. Saving Experimental Parameters or Condition in the Top of Detafile

An exception of FILES MENU is shown in the Table 6-3. The simple explanation is listed in the third column. Before each running, the experimental condition can be recorded in the HEADER LINEs. They will be stored in the first a few lines in the datafile. The mode "Append to existing file" is chosen because we expect to record a set of data with an object at the different bladder volume in one file and each running is separated by HEADER LINES information.

Number of files[0...87]	1	Total number of the files for a run
Current file	1	Identifies the file whose menu page is displayed on the setup screen
Date file name	Aug1$.dat	
Date storage mode	[ASCII Real]	There are 8 data storage modes: e.g. ASCII Integer, Binary Real
Number of header lines	4	Determines the number of header lines to be placed at the beginning of the data file
header line 1,2,3,4	Pig is obstructed for 12 weeks,........	Enter text (experimental condition) for header lines in the file
Date file opening mode	Append to existing file	There are 3 choices: Delete existing file/Append to existing file/Replace records in e isting file
Date file closing mode	End of run	There are 3 options: End of run/After N records/On time of day boundary

Table 6-3: FILES MENU

4. Real-Time Plotting

Experience showed that real-time plotting of data during an experiment, even before a run, is extremely important as a means of ensuring that the experiment was proceeding properly. It can be realized by choose the parameters in the TRACES menu and SCREEN menu. Trace type include: T vs. Y, X vs. Y, horizontal bar, vertical bar, digital meter. SCREEN menu contains the options you use for defining the number and size of windows, window label, tic characteristics, and scroll size.

5. Data Analysis and System Identification

All experimental data files can be 'loaded' in MATLAB for future processing and analyzing.

*R*eferences

REFERENCES

[Bullock, N., G. Sibley and R. Whitaker, 1989] Essential Urology, Churchill Livingstone, New York.

[Brent, L. and F. D. Stephens, 1975] The response of smooth muscle cells in the rabbit urinary bladder to outflow obstruction, Invest. Urol., Vol.12, No.6, 494-502.

[Coolsaet, B. L. R. A., W. A. Van Duyl and R. Van Mastrigt, etc., 1975] Visco-elastic properties of the bladder wall, Urol. Int. 30(1): 16-26.

[Coolsaet, B. L. R. A. 1985] Bladder compliance and detrusor activity during the collection phase, Neurourology and Urodynamics 4: 263-273.

[Griffiths, D., R. V. Mastrigt and R. Bosch, 1989] Quantification of urethral resistance and bladder function during voiding, with special reference to the effects of prostate size reduction on urethral obstruction due to benign prostatic hyperplasia, Neurourology and Urodynamics 8: 17-27.

[Griffiths, D. J., 1977] Urodynamic assessment of bladder function, Br. J. Urol., 49: 29-36.

[Griffiths, D. J., R. Van Mastrigt and W. A. Van Duyl, etc., 1979] Active properties of urinary bladder in the collection phase. Med. Biol. Eng. Comput. 17: 281-290.

[Ghoniem, G. M., C. H. Regnier and P. Biancani, etc. 1985] Effect of vesical outlet obstruction on detrusor contractility and passive properties in rabbits. J. Urol., 135: 1284-1286.

[Gray, H., 1966] Anatomy of the human body, 28th ed. Philadelphia: Lea & Febiger.

[Guan, Z, 1992] A Conscious Minipig Model for Evaluation of the Lower Urinary Tract, Master thesis, Department of Experimental Surgery, McGill University, Montreal, Canada.

[Hill, A. V., 1938] The heat of shortening and the dynamic constants of muscle. Proc. R. Soc. Lond. B Biol. Sci. 126: 136-195.

[Hunter, I. W. and R. E. Kearney, 1982] Dynamics of human ankles stiffness: variation with mean ankle torque, J. Biomech., Vol. 15, No. 10, 747-752.

[Hutch, J. A., 1972] Anatomy and physiology of the bladder, trigone, and urethra, New York: Appleton-Centry-Crofts.

[Igawa, Y., A. Mattiasson and K. E. Andersson, 1992] Is bladder hyperactivity due to outlet obstruction in the rat related to changes in reflexes or to myogenic changes in the detrusor? Acta Physiol Scand, 146(3): 409-411.

[Kearney, R. E., 1992] Peripheral neuromuscular control, Lectural Notes of Selected Topics in Biomedical Engineering, McGill University.

[Kearney, R. E. and I. W. Hunter, 1982] Dynamics of human ankles stiffness: variation with displacement amplitude, J. Biomech. Vol. 15, No. 10, 753-756.

[Kiruluta, G., 1990] Research proposal, Department of Uorology, McGill Univeristy, Canada.

[Kondo, A., J. G. Susset and J. Lefaivre, 1972] Viscoelastic properties of bladder, I. Mechanical model and its mathematical analysis, Invest. Urol., Vol. 10(2): 154-163.

[Kondo, A. and J. G. Susset, 1974] Viscoelastic properties of bladder, II. Comparative studied in normal and pathologic dogs, Invest. Urol. 11(6): 459-465.

[Levin, R. M., J. High and A. L. Wein, 1984] The effect of short-term obstruction on urinary bladder function in the rabbit, J. Urol. Vol. 132(4): 789-791.

[LABTECH, 1991] Notebook reference manu, Laboratory Technologies Corporation, Wilmington, MA.

[Mostwin, J. L., O. M. A. Karim and G. V. Koevering, 1991] The guinea pig as a model of gradual urethral obstruction, J. Urol. 145(4): 854-858.

[Melik, W. F., J. J. Naryka and J. H. Schnidt, 1961] Experimental studies of ureteral peristaltic patterns in the pig: 1. similarity of pig and human urethra and bladder physiology. J. Urol. 85: 145-148.

[Mathworks, 1990] PC-MATLAB user's guide, The Mathworks Inc. Natick, MA.

[Rack, P. M. H., 1966] The behavior of a mammalian muscle during sinusoidal stretching. J. Physiol. 183: 1-14.

[Sibley, G. N. A., 1985] An Experimental model of detrusor instability in the obstructed pig, Br. J. Urol., 57: 292-298.

[Speakman, M. J., A. F. Brading and C. J. Gilpin, etc. 1987] Bladder outflow obstruction -- a cause of denervation supersensitivity. J. Urol. 138: 1461-1466.

[Sbley, G. N. A., 1985] An experimental model of detrusor instability in the obstructed pig, Br. J. Urol. 57: 292-298.

[Schauf, C., D. Moffett and S. Moffett, 1990] Human Physiology: Foundations & Frontiers, St. Louis: Times Mirror/Mosby College Pub..

[Turner, W. R., C. G. Whiteside and E. P. Arnold, etc. 1991] Viscoelastic properties of the contracting detrusor, II. Experimental approach, Am. J. Physiol. 261 (Cell Physiol. 30): C364-C375, 1991.

[Van Mastrigt, R., B. L. R. A. Coolsaet and W. A. Van Duyl, 1978] Passive properties of urinary bladder in the collection phase. Med. Biol. Eng. Comput. 16: 471-482.

[Venegas, J. G., 1991] Viscoelastic properties of the contracting detrusor, I. Theoretical basis, Am. J. Physiol. 260 (Cell Physiol. 31): C355-C363.

[Worth, E. G. J. Milroy and J. R. Webster, etc. 1973] A urodynamic view of prostatectomy, Br. J. Urol. 45: 631-45.

[Woodburne, R. T., 1968] Anatomy of the bladder and bladder outlet, J. Urol. 100: 474-487.